

Uncovering the role of solar radiation and water stress factors in constraining decadal intra-site spring phenology variability in diverse ecosystems across the Northern Hemisphere

Yating Gu¹ , Lin Meng² , Yantian Wang^{3,4} , Zherong Wu⁵ , Yuhao Pan¹ , Yingyi Zhao¹ , Matteo Detto⁶  and Jin Wu^{1,7,8} 

¹Research Area of Ecology and Biodiversity, School of Biological Sciences, The University of Hong Kong, Pokfulam, Hong Kong, China; ²Department of Earth and Environmental Sciences, Vanderbilt University, Nashville, TN 37240, USA; ³Department of Land Surveying and Geo-Informatics, The Hong Kong Polytechnic University, Hung Hom, Hong Kong; ⁴College of Resources and Environment, University of Chinese Academy of Sciences, Beijing, 100049, China; ⁵School of Integrative Plant Science, Soil and Crop Sciences Section, Cornell University, Ithaca, NY 14850, USA; ⁶Department of Ecology and Evolutionary Biology, Princeton University, Princeton, NJ 08544, USA; ⁷Institute for Climate and Carbon Neutrality, The University of Hong Kong, Pokfulam, Hong Kong, China; ⁸State Key Laboratory of Agrobiotechnology, The Chinese University of Hong Kong, Hong Kong, SAR China

Summary

Author for correspondence:

Jin Wu

Email: jinwu@hku.hk

Received: 11 December 2024

Accepted: 12 March 2025

New Phytologist (2025) 246: 1986–2003

doi: 10.1111/nph.70104

Key words: climate change, optimality strategy, photoperiod, solar radiation, spring phenology, temperature, water stress.

- The spring phenology has advanced significantly over recent decades with climate change, impacting large-scale biogeochemical cycles, climate feedback, and other essential ecosystem processes. Although numerous prognostic models have been developed for spring phenology, regional analyses of the optimality (OPT) strategy model that incorporate environmental variables beyond temperature and photoperiod remain lacking.
- We investigated the roles of solar radiation (SR) and three water stress factors (precipitation (P), soil moisture, and vapor pressure deficit (VPD)) on spring phenology from 1982 to 2015 using the OPT model with Global Inventory Modeling and Mapping Studies NDVI3g dataset and environmental data from TerraClimate, CRU_TS, and Global Land Data Assimilation System across the Northern Hemisphere (> 30°N).
- Our results show that SR and water stress factors significantly impacted intrasite decadal spring phenology variability, with water stress factors dominant in grassland ecosystems while SR dominated in the rest of the ecosystem types. Enhanced models incorporating SR (OPT-S) and VPD (OPT-VPD) outperformed the original OPT model, likely due to improved representation of the adaptive strategy of spring phenology to optimize photosynthetic carbon gain while minimizing frost risk.
- Our research enhances the understanding of the key environmental drivers influencing decadal spring phenology variation in the Northern Hemisphere and contributes to more accurate forecasts of ecological responses to global environmental change.

Introduction

Spring phenology in the Northern Hemisphere marks the onset of leaf development and plays a critical role in regulating various terrestrial surface biophysical and biochemical processes. These processes include changes in land surface albedo, land-atmosphere carbon and water exchanges, forest productivity, and nutrient cycling (Fang *et al.*, 2020; Gerst *et al.*, 2020; Huang *et al.*, 2023). Additionally, spring phenology influences numerous biotic interactions, such as intra- and interspecies competition for resources and trophic interactions with other living organisms (Cohen & Satterfield, 2020). Furthermore, vegetation-mediated climate feedback is impacted by spring phenology, as it can lead to earlier soil water depletion (Lian *et al.*, 2020) and an increased risk of summer droughts (Vitasse

et al., 2021; Li *et al.*, 2023). Despite the importance of spring phenology in ecological and Earth surface processes, our understanding of the drivers behind its variability across large vegetated landscapes and extended periods remains incomplete, creating considerable amounts of uncertainty when estimating how future climate change will affect spring phenology and other related biological processes (Geng *et al.*, 2020; Xie & Wilson, 2020; Adams *et al.*, 2021).

To better understand and represent the mechanisms underlying plant spring phenology in response to climate change, researchers have developed numerous prognostic models, such as growing degree day (GDD) models, sequential models, and parallel models (McMaster & Wilhelm, 1997; Melaas *et al.*, 2016; Zhao *et al.*, 2021). These models incorporate key environmental indicators, such as temperature and photoperiod, to predict the

leaf unfolding data (LUD) and other phenological timing (Chuine *et al.*, 2000, 2013). The majority of these models attribute phenological shifts to chilling, that is, the exposure of plants to cold temperatures to break dormancy, forcing, which involves exposure to warm temperatures, and the photoperiod effect to promote growth (Heide, 2003; Schwartz *et al.*, 2006). In addition to these models that only consider temperature and photoperiod, researchers recently have developed the eco-evolutionary optimality (OPT) theory and associated OPT-based spring phenology model as a more comprehensive and innovative hypothesis for spring phenology modeling (Fu *et al.*, 2020; Wang *et al.*, 2020b; Meng *et al.*, 2021). This theory posits that the LUD in plants results from trade-offs aimed at maximizing photosynthetic carbon gain and minimizing frost risk. This hypothesis was supported by Gu *et al.* (2023), who analyzed data from hundreds of temperate ecosystem sites in the north and east of the United States, highlighting the significant, yet overlooked role of solar radiation (SR) in having a greater impact on early-season plant photosynthesis potential than photoperiod. These prognostic models have significantly enhanced our ability to quantify phenology shifts in response to climate change, therefore improving the assessments of how these shifts impact various ecosystem processes and functions, such as carbon, water, and nutrient cycles (Nord & Lynch, 2009; Buermann *et al.*, 2018; Lian *et al.*, 2020; Zhou *et al.*, 2022), as well as related climate change feedback (Richardson *et al.*, 2013; Shen *et al.*, 2015).

Despite these advancements in our understanding and modeling of spring phenology, key knowledge gaps remain. First, most prior large-scale assessments of prognostic phenology models have primarily concentrated on a narrow range of environmental variables, such as temperature and photoperiod (Singh *et al.*, 2017; Richardson *et al.*, 2018b; Meng *et al.*, 2021), neglecting other influential environmental variables. For instance, variables such as soil moisture (SM) and vapor pressure deficit (VPD), which affect plant water availability and transpiration, have demonstrated an impact on the timing of leaf unfolding and other phenological events (Li *et al.*, 2021; Zhang *et al.*, 2021), yet receive inadequate attention in current models. Similarly, SR, which drives plant photosynthesis and growth, also impacts phenology (Z. Ren *et al.*, 2022; Gu *et al.*, 2023). This omission makes the mechanisms and modeling underlying large-scale spring phenology incomplete. Second, recent efforts focusing on more environmental variables were often confined to a select number of sites within the United States (e.g. Gu *et al.*, 2023). It remains unknown whether these findings can be extended to large, spatially continuous landscapes over the entire Northern Hemisphere. Furthermore, several empirical studies have reported various environmental variables on water stress conditions, such as precipitation (P) (Ganjurjav *et al.*, 2020), SM (Tao *et al.*, 2020), and VPD (Grossiord *et al.*, 2020). These variables can influence spring phenology in temperate ecosystems, and their relative importance often varies with different plant functional types (PFTs) (Nemani, 2003; Caldararu *et al.*, 2016). This implies a more complex regulation mechanism of spring

phenology in temperate ecosystems than that which is included in state-of-the-art prognostic models. In other words, it remains unclear whether the variables represented in current models are comprehensive and if the dominant environmental variables would vary with different PFTs (Hmimina *et al.*, 2013; Ji *et al.*, 2021). Should such variability across PFTs exist, identifying the overarching mechanisms that account for the diversity in the phenology–environmental cue relationship across broader landscapes becomes crucial and warrants immediate exploration.

Several recent technical advances offer a unique and timely opportunity to bridge the aforementioned knowledge gaps: the availability of long time-series phenology datasets covering the entire Northern Hemisphere (Friedl *et al.*, 2019; Zhang *et al.*, 2020) and the recently developed diagnostic approach for exploring the potential impact of comprehensive environmental variables on spring phenology modeling (Gu *et al.*, 2023). One typical example of this long-term phenology dataset is the LUD extracted from the Global Inventory Modeling and Mapping Studies (GIMMS) NDVI3g dataset (C. Wu *et al.*, 2022); this dataset is developed based on algorithms retrieving the phenology transition dates, providing us not only extensive spatial coverage (i.e. the entire Northern Hemisphere) but also covering a long time duration (i.e. 1982–2015). Concurrently, Gu *et al.* (2023) developed a holistic analytical framework that not only examined the performance of existing prognostic models for spring phenology modeling but also established a quantitative pipeline that assessed the partial correlation between the model residuals and other environmental variables not yet included in the current models, by which the effectiveness and the most sensitive variable would be identified. As a result, we expect that the integration of these two advances will provide relevant quantitative results across the entire Northern Hemisphere, helping to address the key knowledge gaps identified earlier.

This study thus aims to assess and improve the existing model of spring phenology (e.g. the OPT model introduced in Meng *et al.*, 2021) for intrasite decadal spring phenology modeling across the entire Northern Hemisphere by exploring other variables beyond temperature and photoperiod. Specifically, we address three key questions: (1) How does the OPT model perform in simulating spring phenology on a hemispheric scale? (2) What are the key environmental variables responsible for intrasite model residuals, and whether these variables differ across PFTs? (3) How significantly can the new prognostic models enhance spring phenology modeling? To answer these questions, we used satellite land surface phenology products and environmental datasets over the Northern Hemisphere for the years 1982–2015. We trained and evaluated the existing OPT model developed by Meng *et al.* (2021), which has demonstrated superior model performance compared with other prognostic models of GDD models and sequential models (Gu *et al.*, 2023). Given that the hemisphere-scale spring phenology dataset has a coarse spatial resolution of 1/12° and long-term data often come with significant climate anomalies, we further investigated whether

landscape PFT heterogeneity and climate anomalies contribute to the model residuals. Subsequently, the relationships between the model residuals and climate variables were examined, including SR and three water stress factors: P, SM, and VPD. This analysis aimed to identify additional environmental factors, not accounted for in current models, that have a substantial impact on the variability of spring phenology, and to determine whether the dominant environmental variable varies across PFTs. Last, we revised the OPT model by incorporating the identified dominant environmental variable(s) and investigated whether these revisions could enhance the model's performance.

Materials and Methods

Study area and PFTs

This research focused on the North Hemisphere and excluded subtropical regions (i.e. latitudes lower than 30°N) due to their more subtle seasonality in vegetation greenness and the more complex mechanisms underlying their phenological regulations (Liu *et al.*, 2016). The study area is predominantly located within the temperate climate zone, which accounts for 73.09% of the region according to the Köppen climate classification (Beck *et al.*, 2018; Supporting Information Fig. S1; Table S1). This zone is characterized by well-defined seasonal patterns in vegetation dynamics, making it ideal for analyzing phenological responses. We used the HILDA+ annual land use/cover dataset, which has a 1 km spatial resolution (Winkler *et al.*, 2020), to exclude pixels dominated by Urban, Cropland, and Pasture, given the strong influence of human activities (Ma *et al.*, 2022). We also excluded nonvegetation areas referred to as 'Other land' and 'Water'.

In our study, we established a criterion to assign a pixel's PFT, requiring the dominant PFT proportion to be > 50% for a period exceeding 80% between 1982 and 2015; otherwise, the pixel was excluded from the analysis. Due to its relatively small overall fraction, the evergreen broadleaf forest area was also excluded from our analysis. Consequently, we selected six dominant land cover types for our study: Grass/Shrubland (GSL), which constitutes 39.61% of the study area, followed by evergreen needleleaf forest (ENF; 25.86%), deciduous needleleaf forest (DNF; 20.18%), deciduous broadleaf forest (DBF; 9.00%), mixed forest (MXF; 4.04%), and unknown/other forest (UOF; 1.24%).

Datasets

To investigate the large-scale spring phenology pattern while minimizing data uncertainty, several remote sensing data resources were utilized, including LUD derived from a 15-d NDVI time series product of the GIMMS from the Advanced Very High-Resolution Radiometer. Additionally, we used climate datasets including temperature and SR from the Global Land Data Assimilation System (GLDAS), as well as water availability

indicators (SM and VPD) from TerraClimate and precipitation from CRU_TS v4.03 for the period 1982–2015. Notably, we selected these climate datasets not only because they provided long time series but also because they offered relatively higher spatial resolution. To maintain a balance between spatial resolution consistency and heterogeneity effects, all data were resampled to a 1/12° resolution using a 2 × 2 nearest neighbor interpolation method.

Satellite-derived LUD data We utilized satellite LUD data for the Northern Hemisphere (> 30°N) from 1982 to 2015, with a spatial resolution of 1/12° (C. Wu *et al.*, 2022). This data was derived from the 15-d NDVI time series of the GIMMS NDVI3g dataset (NASA GIMMS, 2015). After preprocessing and quality control of the original NDVI time series data, LUD was extracted using the average of three methods: (1) the dynamic-threshold method (White *et al.*, 2009), (2) a piecewise logistic function (Zhang *et al.*, 2003), and (3) a modified double-logistic function (Gonsamo *et al.*, 2012). There are two main reasons for selecting this phenology dataset. First, by using the average of the three methods, the data has demonstrated significantly reduced uncertainty and improved consistency over time (C. Wu *et al.*, 2022). Second, the dataset has shown improved accuracy when compared with ground and phenocam data (Liu *et al.*, 2023).

Climatic datasets To investigate the potential influence of water stress factors on the spring phenology model's residuals, we employed three water stress indicators, including SM, P, and VPD. For SM and VPD, we obtained monthly SM (mm) and VPD (kPa) for 1982–2015 from TerraClimate (Abatzoglou *et al.*, 2018) with a spatial resolution of 1/24°. For precipitation data, we derived monthly P data (mm per month) with a spatial resolution of 0.5° from the CRU_TS v4.03 product (Harris *et al.*, 2020). For temperature and SR data from 1982 to 2015, we used the NASA GLDAS (NASA GES DISC, 2023). The spatial and temporal resolutions of these data are 0.25° and a 3-h interval, respectively. Using this dataset, we calculated the average daily temperature and aggregated daily SR as inputs for the spring phenology model.

Methodology

Model description In this study, we employed the OPT strategy model. This model was established in accordance with the eco-evolutionary theory (Meng *et al.*, 2021), which posits that plants adopt optimal strategies for their spring phenology to maximize carbon gain from photosynthesis while simultaneously reducing the risk of frost damage (Chamberlain & Wolkovich, 2021).

To be specific, the date t marks the LUD when the potential photosynthetic carbon benefit is larger than the impact of the potential frost damage risk, that is,

$$F_t \geq ae^{-bC_t} \quad \text{Eqn 1}$$

where C_t and F_t are the accumulated chilling and forcing from t_0 (empirically set as the first day of the calendar year) to t . C_t and F_t are computed as follows:

$$C_t = \sum_{i=t_0}^t R_{c,i} \quad \text{Eqn 2}$$

$$F_t = \sum_{i=t_0}^t R_{f,i} \times R_{p,i} \quad \text{Eqn 3}$$

where $R_{c,i}$, $R_{f,i}$, and $R_{p,i}$ are the rates of chilling, forcing, and realized forcing in the i^{th} day.

Since temperature influences chilling and forcing under different circumstances, OPT captures the chilling effect according to the triangular function (Richardson *et al.*, 1974; Chuine *et al.*, 2000; Melaas *et al.*, 2016), expressed as

$$R_{c,i} = \begin{cases} 0 & T_i < T_{\min} \\ \frac{T_i - T_{\min}}{T_{\text{opt}} - T_{\min}} & T_{\min} \leq T_i < T_{\text{opt}} \\ \frac{T_i - T_{\text{opt}}}{T_{\max} - T_{\text{opt}}} & T_{\text{opt}} \leq T_i < T_{\max} \\ 0 & T_i > T_{\max} \end{cases} \quad \text{Eqn 4}$$

where T_i is the average temperature of the i^{th} day, $T_{\min} = -5^{\circ}\text{C}$, $T_{\text{opt}} = 10^{\circ}\text{C}$, and $T_{\max} = 25^{\circ}\text{C}$, based on Wang *et al.* (2020b).

A sigmoid function is used to compute the forcing rate (Meng *et al.*, 2021):

$$R_{f,i} = \begin{cases} 0, & T_i \leq T_{\text{base}} \\ \frac{28.4}{1 + \exp(3.4 - 0.185 T_i)} & T_i > T_{\text{base}} \end{cases} \quad \text{Eqn 5}$$

where $T_{\text{base}} = 5^{\circ}\text{C}$ is the temperature threshold for biological activity.

Finally, the state of realized forcing (Meng *et al.*, 2021) is given by

$$R_{p,i} = \frac{L_i}{12} e^{-c R_{c,i}} \quad \text{Eqn 6}$$

where L_i is the day length of the i^{th} day. The model has three fitting parameters: a , b , and c .

In addition to the OPT model, we also examined other prognostic models for large-scale spring phenology modeling, including GDD and sequential models, following the approach of Gu *et al.* (2023). However, we found that these models consistently underperformed compared to the OPT model, as demonstrated by Gu *et al.* (2023). Therefore, to simplify the presentation, we focused exclusively on the OPT model in this paper.

Model accuracy assessment and validation To ensure the robustness of model training, we adopted a 5-fold cross-validation method with 20 repetitions, as suggested by Yan *et al.* (2021). We evaluate the OPT model on a pixel-by-pixel

basis, using environmental factors and LUD extracted from satellite data as inputs. Each pixel had a data record spanning from 1982 to 2015 ($n = 34$ yr). Following C. Wu *et al.* (2022), we employed three metrics for model performance evaluation: root mean square error (RMSE), Kling–Gupta efficiency (KGE) (Gupta *et al.*, 2009), and Pearson's correlation coefficients (R). Notably, KGE was adopted because it provides a balanced assessment by incorporating correlation, bias, and the ratio of variances. This approach eliminates the need for reference forecasts or simulations, resulting in more interpretable and meaningful values or scores for modelers (Liu, 2020).

Heterogeneity and climate anomaly Since our phenology analysis and modeling were performed at a $1/12^{\circ}$ resolution, most of the examined pixels contained a mosaic of multiple PFTs. To explore the potential impact of these spatial mosaics of different PFTs (Liu *et al.*, 2019; Ren *et al.*, 2022a) on the OPT model residuals, we examined the relationship between the model RMSE and two metrics that indicate the level of PFT heterogeneity within each pixel (corresponding to a specific vegetated landscape). These metrics are (1) the proportion of the dominant PFT, which was determined by calculating the average value of the dominant PFT over a 34-year period (using the HILDA+PFT product) within a $1/12^{\circ}$ grid cell, and (2) the entropy of the PFT mosaic, which was calculated using Eqn 7 as a measure of randomness or disorder within a pixel.

$$\text{Entropy} = - \sum_{i=1}^n p_i \log_2(p_i) \quad \text{Eqn 7}$$

where p_i indicates the 34-year averaged proportion of each PFT, and n indicates the number of PFTs contained in each pixel.

To investigate the effects of climate anomalies, we first divided the 34-year data for each pixel into five climate ranges, such as $(-\infty, \bar{T} - 2\sigma_T)$, $[\bar{T} - 2\sigma_T, \bar{T} - \sigma_T)$, $[\bar{T} - \sigma_T, \bar{T} + \sigma_T)$, $[\bar{T} + \sigma_T, \bar{T} + 2\sigma_T)$, and $[\bar{T} + 2\sigma_T, +\infty)$, where \bar{T} and σ_T are the mean and SD of a specific pixel's 34-year temperature anomaly. Second, to assess the extent to which climate anomaly conditions might influence model performance in each climate range, we calculated the mean absolute error (MAE), which assigns relatively lower weight to errors compared to RMSE, between the validation data and the model results (Gupta *et al.*, 2009). Third, we used ANOVA to compare the means among the five groups (Park, 2009). If the P -value of the ANOVA was significant, it would indicate that at least one pair had a statistically significant difference from the other groups.

Evaluating model residuals in conjunction with additional environmental factors In order to investigate the potential impact of unaccounted environmental factors on the variability of spring phenology in existing predictive models, we initially calculated the residuals between the model results and satellite-derived data (i.e. the difference between modeled and observed LUD). Subsequently, we analyzed the associations between these residuals and the average values of VPD_{pre}, precipitation (P_{pre}), SM_{pre}, and SR_{pre} during the period preceding the

LUD or preseason. For each environmental variable, we followed Gu *et al.* (2023) and determined the preseason (with a 30-d duration) by identifying the time interval with the greatest correlation between the environmental factor and LUD from 1982 to 2015. Subsequently, we utilized partial correlation analysis as a method to examine the dependence of model residuals on each of the four indicators while constraining the impacts of the other three indicators (Liu *et al.*, 2016).

After deriving variable-specific partial correlation coefficients and considering that VPD, P, and SM can all indicate plant water stress, we conducted an additional analysis to determine the dominant environmental variables (related to light and water) for the model residual: (1) A region is identified as a light-constrained region if the partial correlation of SR_{pre} (P_{C-SR}) > 0, indicating that higher SR advances LUD (Z. Wu *et al.*, 2022), and the absolute partial correlation coefficient of SR_{pre} is higher than that of water stress factors; (2) A water-constrained region is identified if water stress factors negatively/positively correlate with spring phenology (i.e. P_{C-P} > 0, P_{C-SM} > 0, or P_{C-VPD} < 0) and the absolute partial correlation strength of that specific water stress factor is higher than that of SR_{pre} ; (3) for other cases (e.g. P_{C-P} < 0, P_{C-SM} < 0, P_{C-SR} < 0, or P_{C-VPD} > 0), we considered that the partial correlation result for that specific environmental factor might be caused by various uncertainties (e.g. data error, indirect correlation with other environmental factors like temperature or others, and thus representing an apparent effect rather than true physiological constraint of these factors on approximating early growing season plant photosynthetic potential). As a result, we only retained those effective partial correlations and assigned them as either dominantly constrained by light or water based on their absolute strength.

Revised phenology models and model assessment Once the most important environmental variable(s) influencing the model residuals have been identified, we proceeded to integrate these missing environmental cues into the current OPT model. This approach aimed to explore the potential for enhancing spring phenology model performance. We presented two revised versions of OPT as below.

OPT-S model. Similar to Gu *et al.* (2023), our subsequent analysis identified SR_{pre} as one of the most important environmental variables contributing to the model residual. Thus, we followed Gu *et al.* (2023) and used Eqn 8, which replaces photoperiod L_i with SR_{pre} to account for the SR_{pre} effect on spring phenology modeling. The theory underlying this revision is likely because that SR is a more efficient variable than photoperiod in signaling the potential photosynthetic carbon gain during the period of leaf emergence (Badeck *et al.*, 2004; Yang *et al.*, 2022).

$$R_{p,t} = (SR_t - SR_0) e^{-cR_{c,t}} \quad \text{Eqn 8}$$

where SR_t and SR_0 denote the solar radiation on date t and the constant threshold of solar radiation, respectively. The threshold (SR_0) is applicable to all sites and serves to mitigate the influence

of the variations in the absolute value of solar radiation, thereby eliminating the magnitude differences constrain F_t in Eqn 3.

OPT-VPD model. In addition to SR, our subsequent analysis identified VPD as another crucial variable responsible for the model residuals. Although all three water stress metrics (i.e. P, SM, and VPD) were observed to affect spring phenology, our later results indicate that VPD has the most significant impact (see ‘Dominant environmental variables of light and water for spring phenology modeling across different PFTs’ in the Results section). Meanwhile, compared to the other two factors, VPD has a clearer and more easily modeled influence on growing season plant photosynthesis potential (e.g. Wang *et al.*, 2025), while focusing on the most critical factor, VPD, rather than including all three factors, simplifies the modeling process and facilitates the hypothesis testing. Thus, we revised the OPT model to account for the VPD effect in constraining spring phenology modeling. We modified the OPT model to create the OPT-VPD model, which included V_{crit} as a VPD constraint that was linearly correlated with preseason VPD. The LUD criteria (i.e. Eqn 9) were formulated by the following equation:

$$F_t \times V_{crit} \geq ae^{-bC_t} \quad \text{Eqn 9}$$

with

$$V_{crit} = 1 - d \times VPD_{pre} \quad \text{Eqn 10}$$

where VPD_{pre} represent the preseason VPD average for the month of t , and the model has four fitting parameters a , b , c , and d .

Notably, we also attempted to create an ‘OPT-S-VPD’ model that considers both SR and VPD, exploring its potential benefits over individual ‘OPT-S’ or ‘OPT-VPD’ models. However, our observations indicated that the combined model did not perform as well as the individual models (Fig. S2). This outcome is likely due to the strong collinearity between SR and VPD, as higher SR often correlates with higher temperatures, leading to increased VPD. Given that SR positively influences plant photosynthesis, whereas VPD negatively impacts it, modeling both SR and VPD simultaneously presents challenges. Therefore, in the main text, we primarily focused on the ‘OPT-S’ and ‘OPT-VPD’ models. We do, however, acknowledge in the Discussion section that future modeling efforts should aim to comprehensively account for both SR and VPD effects using more advanced prognostic models.

Statistical analysis To assess the effectiveness of the revised models, we employed two methods to evaluate their efficiency and test the underlying hypothesis. First, we examined whether the modified models could yield notable model improvements using RMSE as the performance metric, particularly compared to the original models that utilized temperature and photoperiod as input factors. Second, to ensure that the improvement does not come at the expense of escalating model residuals to other variables, we computed the significant Pearson partial correlation

(P -value < 0.05) again for the residuals derived from the revised model. The same approach was also applied to calculate the partial correlation between model residuals and environmental variables.

Results

Evaluation of the prognostic model's effectiveness in modeling spring phenology

The default OPT model across the entire Northern Hemisphere had a median RMSE of 7.08 d (Fig. 1a,d) and the performance was also consistent across metrics, with KGE and R showing similar patterns (Fig. 1b,c). There was a significant degree of variability in these performance metrics across the entire Northern Hemisphere. The RMSE values ranged from 5.26 (first quartile with the value under 25% of data points Q1: 25%) to 8.96 (third quartile with the value under 75% of data points Q3: 75%) days (Fig. 1a,d). The KGE values (Fig. 1b,e) ranged from 0.36 (Q1: 25%) to 0.71 (Q3: 75%), with a median value of 0.56, whereas the R values (Fig. 1c,f) ranged from 0.52 (Q1: 25%) to 0.82 (Q3: 75%), with a median value of 0.71.

Next, we examined the model performance at the PFT level and found that the results displayed some degree of variability depending on the specific PFT of interest. Fig. 1(d) shows that DNF exhibited the best model performance, with a median RMSE of 6.31 d. Mixed forest ranked second with an RMSE of 6.67 d, followed by GSL (6.93 d), DBF (7.61 d), ENF (7.95 d), and UOF (8.41 d). Similar observations were also found using the other two performance metrics of KGE and R . Satellite-derived (Fig. 1g–j) and model-predicted (Fig. 1k–n) phenology of selected years (1985, 1995, 2005, and 2015) corresponded well with each other both across space and time, suggesting no significant systematic biases in the model-predicted phenology results (also refer inserted subplots in Fig. 1k–n).

Although the default OPT model demonstrated reasonably good accuracy in capturing spring phenology across the North Hemisphere, we also observed considerable model residual variations across large landscapes, encompassing nearly all climate spaces of mean annual temperature and mean annual precipitation as well as key PFTs (Fig. 2a). Further quantitative analysis indicated that 21.55% of land area across the entire Northern Hemisphere had an RMSE of 0–5 d, 62.03% of land areas had an RMSE of 5–10 d, 9.78% had an RMSE of 10–15 d, and 6.64% had an RMSE of > 15 d (Fig. 2b).

Exploring the model residual and its association with other factors

We next investigated factors that might influence the residuals of the trained OPT model. We proposed three hypotheses to explain the residual variation in the model: (1) heterogeneity in PFTs at the pixel level, (2) interannual climate anomalies, particularly extreme temperature events (e.g. unusually cold or hot conditions), and (3) additional environmental factors beyond temperature and photoperiod that are not accounted for in the

current OPT model. Our findings supported the third hypothesis, indicating that these unrepresented environmental variables play a significant role, while the first two hypotheses were barely supported (Fig. S3).

Specifically, when examining Hypothesis 1, we assessed pixel-level PFT heterogeneity using two metrics: the 34-years mean proportion of dominant PFT (Fig. S3a–d) and PFT entropy (Fig. S3e–h). The analysis focused on the four most abundant PFTs: ENF, DBF, MXF, and GSL. The results demonstrated minimal to no correlation between both PFT heterogeneity metrics and the RMSE for all evaluated PFTs. The correlation coefficients for the proportion mean of dominant PFT were 0.05 for ENF, 0.08 for DBF, -0.02 for MXF, and -0.04 for GSL (P -values < 0.05). The correlation coefficients for entropy were -0.03 for ENF, -0.07 for DBF, 0.04 for MXF, and 0.04 for GSL, with all P -values < 0.05 . These findings suggest that pixel-level PFT heterogeneity does not have a significant impact on the model residuals. Regarding Hypothesis 2, we used the MAE metric to examine the effect of climate anomalies on model residuals relative to normal climatic conditions. Interestingly, years with climate anomalies such as $(-\infty, \bar{T} - 2\sigma_T)$ and $(\bar{T} + 2\sigma_T, +\infty)$ did not exhibit any noticeable difference in the distribution of data compared to normal years (P -value = 0.09), indicating that the model operates nearly as effectively under extreme conditions (Fig. S3i).

We tested Hypothesis 3 by analyzing the partial correlation coefficients between the model residuals and the preseason environmental variables, namely P_{pre} , SM_{pre} , SR_{pre} , and VPD_{pre} (Fig. 3). Our results show that the strength and sign of partial correlation coefficients vary significantly across the four variables examined as well as exhibit strong spatial heterogeneity across the entire study region. When focusing on the partial correlation of P_{pre} (Fig. 3a), large variations were observed across different PFTs. DBF showed a correlation coefficient (mean \pm SD) of 0.37 ± 0.41 , DNF of -0.36 ± 0.41 , ENF of -0.32 ± 0.43 , GSL of -0.34 ± 0.34 , MXF of 0.37 ± 0.43 , and UOF of -0.35 ± 0.41 . Similar observations also applied to the other two plant water stress metrics, that is SM_{pre} (Fig. 3b) and VPD_{pre} (Fig. 3d). By contrast, the partial correlation of SR was relatively more consistent across different PFTs (Fig. 3c), with the correlation coefficients of 0.42 ± 0.41 for DBF, 0.42 ± 0.36 for DNF, 0.41 ± 0.41 for ENF, 0.28 ± 0.40 for GSL, 0.43 ± 0.36 for MXF, and 0.39 ± 0.42 for UOF.

Based on the variable-specific partial correlation coefficient results presented in Fig. 3, along with the ecological criteria proposed for identifying regions dominated by light vs water stress (see 'Evaluating model residuals in conjunction with additional environmental factors' in the Methodology section), we mapped the vegetated landscapes where model residuals were most sensitive to P_{pre} , SM_{pre} , SR_{pre} , and VPD_{pre} , respectively (Fig. 4). From these newly derived maps, we observed that SR_{pre} dominated 55.46% of the entire study area, followed by VPD_{pre} (21.27%), P_{pre} (14.80%), and SM_{pre} (8.47%). Notably, we observed more consistent partial correlation coefficient signs this time. The partial correlation coefficient of P_{pre} peaked at MXF with 0.33 ± 0.10 and reached a minimum at UOF with 0.29 ± 0.10 .

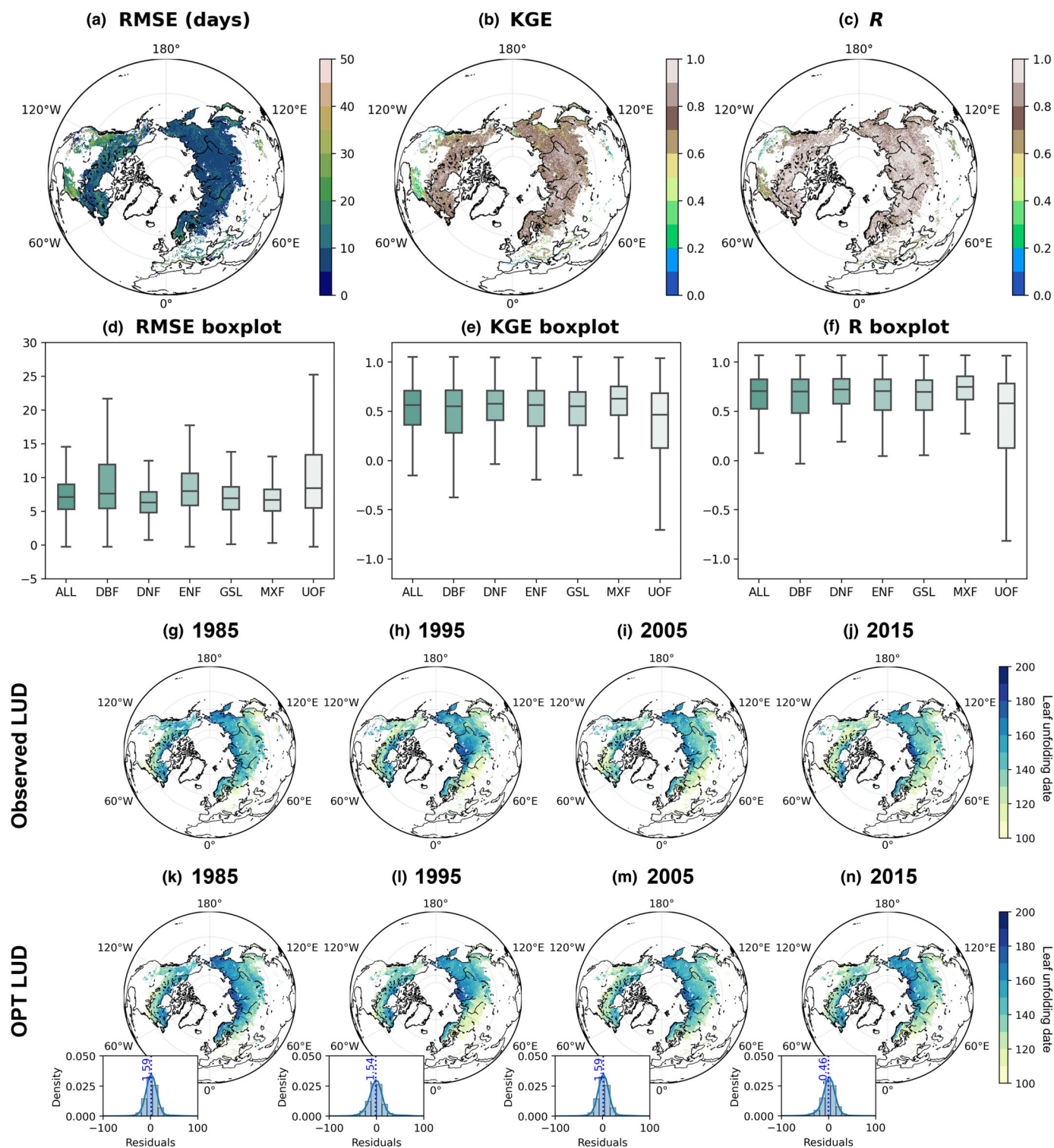


Fig. 1 The overall performance of the prognostic optimality (OPT) strategy model in modeling plant spring phenology and performance summary across plant functional types (PFTs) (grass/shrubland (GSL): 39.61%; evergreen needleleaf forest (ENF): 25.86%; deciduous needleleaf forest (DNF): 20.18%; deciduous broadleaf forest (DBF): 9.00%; mixed forest (MXF): 4.04%; unknown/other forest (UOF): 1.24%), using the three accuracy metrics of RMSE (a, d), KGE (b, e), R (c, f), where the box spans from the first quartile (Q1) to the third quartile (Q3), with a line marking the median and the whiskers extend to the farthest data point within 1.5 times the interquartile range (IQR) from the box; spatial and temporal patterns of spring phenology from the OPT model (g–n) compared with those from the Global Inventory Modeling and Mapping Studies (GIMMS) NDVI3g dataset (g–j) in the selected years: 1985, 1995, 2005, and 2015. The inserted figures in (k–n) indicates the distribution of model residuals (i.e. modeled leaf unfolding date (LUD) minus satellite-derived LUD), where the blue dashed line shows the mean value of the histogram. RMSE, root mean square error; KGE, Kling–Gupta efficiency; R, Pearson's correlation coefficients; ALL, all the plant functional types.

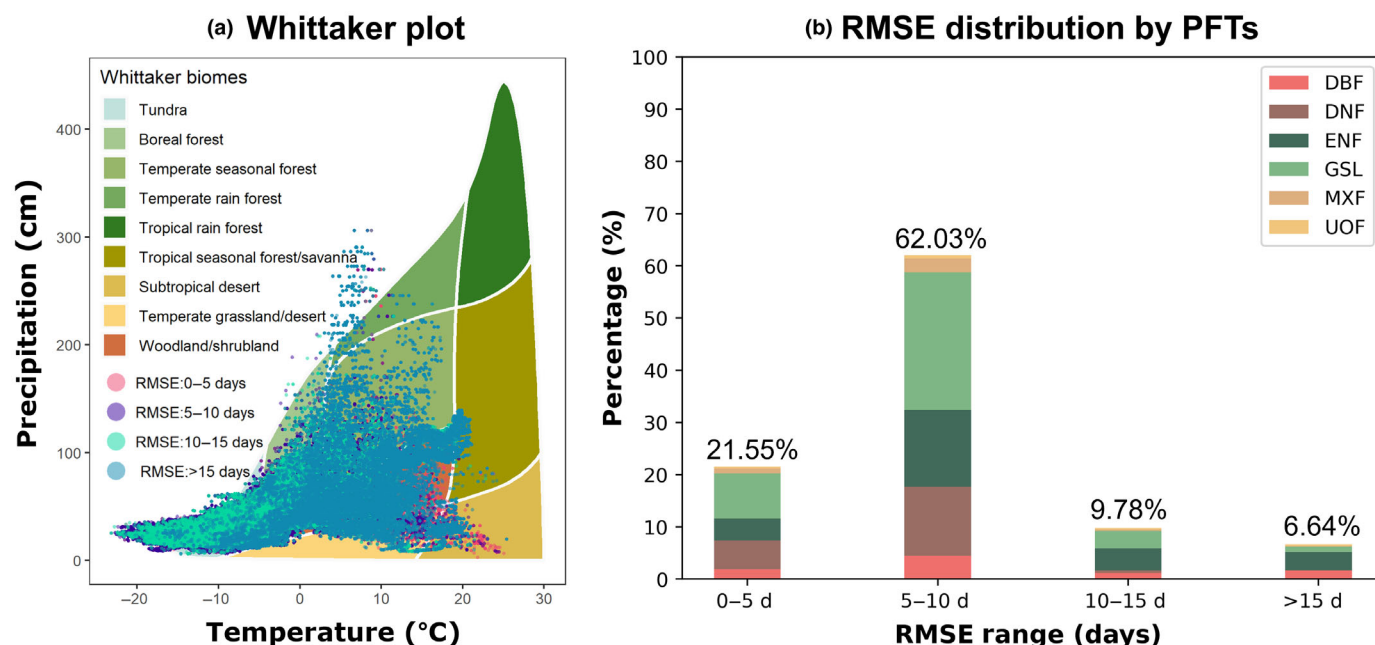


Fig. 2 Evaluation of the optimality (OPT) model's performance across climatic gradients and plant functional types (PFTs). (a) Whittaker plot depicting the correlation between precipitation, temperature, and the root mean square error (RMSE) distribution of the OPT for different intervals (0–5 d, 5–10 d, 10–15 d, and > 15 d). (b) The RMSE distribution across different PFTs. DBF, deciduous broadleaf forest; DNF, deciduous needleleaf forest; ENF, evergreen needleleaf forest; GSL, grass/shrubland; MXF, mixed forest; UOF, unknown/other forest.

(Fig. 4a). The partial correlation coefficient of SM_{pre} peaked at MXF with 0.33 ± 0.11 and reached a minimum at DNF with 0.29 ± 0.12 (Fig. 4b); the partial correlation coefficient of SR_{pre} peaked at ENF with 0.45 ± 0.13 and reached a minimum at GSL with 0.30 ± 0.11 (Fig. 4c). Finally, the partial correlation coefficient of VPD_{pre} peaked at DNF with -0.34 ± 0.10 and reached a minimum at DBF with -0.38 ± 0.10 (Fig. 4d).

Dominant environmental variables of light and water for spring phenology modeling across different PFTs

We next examined the influence of light vs water on spring phenology modeling across various PFTs. To do this, we incorporated three factors – P_{pre} , SM_{pre} , and VPD_{pre} – that indicate water stress on spring phenology regulation. Along with SR_{pre} , we analyzed the dominance of light vs water stress in affecting spring phenology. Our results, which illustrate the composite of light vs water stress on spring phenology modeling, are shown in Fig. 5(a), where the light-dominated area accounts for 55.46% of all study areas, and the remaining area is water-dominated. By integrating the hemisphere scale-dominant climate stress map (Fig. 5a) with the relevant PFT map (Fig. 5b), we further assessed the portion of light- vs water-dominated areas at the PFT level. Our results (Fig. 5c) show that both light and water stress coexist in all examined PFTs. Grass/Shrubland is predominantly influenced by water stress-related environmental variables, with nearly three times more water-constrained regions compared with those constrained by light availability (light: 11.32%; water: 28.30%). By contrast, all other PFTs are dominated by SR, with nearly twice as many light-constrained regions compared to those

constrained by water stress. Focusing on the water-constrained regions, we found that all three water stress metrics – P_{pre} , SM_{pre} , and VPD_{pre} – play a role in affecting spring phenology modeling, a pattern consistent across all examined PFTs (Fig. 5d).

Examining the revised models' performance and their residual connections with key environmental variables

Having identified light (i.e. SR) and dominant water stress (i.e. VPD) factors as responsible for model residuals in the default OPT model, we investigated whether the revised OPT model incorporating SR or VPD would improve the prognostic modeling of spring phenology over the Northern Hemisphere. Our results revealed a consistent pattern across all three performance metrics analyzed, as well as at both the all-site and PFT levels for evaluation. The default OPT model had the lowest model performance, while the revised OPT-S model showed the highest performance, and the revised OPT-VPD model fell in between both (Fig. 6a–c). Taking RMSE as an example, at the all-site level, we observed a 42.79% reduction in RMSE for OPT-S (RMSE = 4.05 d) and an 11.59% reduction in RMSE for OPT-VPD (RMSE = 6.26 d) relative to the default OPT (RMSE = 7.08 d). At the PFT level, the model performance improved the most for OPT-S (a 46.25% reduction in RMSE relative to the default OPT) in DBF and the least (a 39.05% reduction in RMSE) in UOF, whereas other PFTs, such as DNF, MXF, GSL, and ENF, fell in between. Similarly, we observed the model performance improved the most (a 30.11% reduction in RMSE) for OPT-VPD in DBF, the least (a 6.40% reduction in RMSE) in GSL, and other PFTs, such as UOF, MXF, and

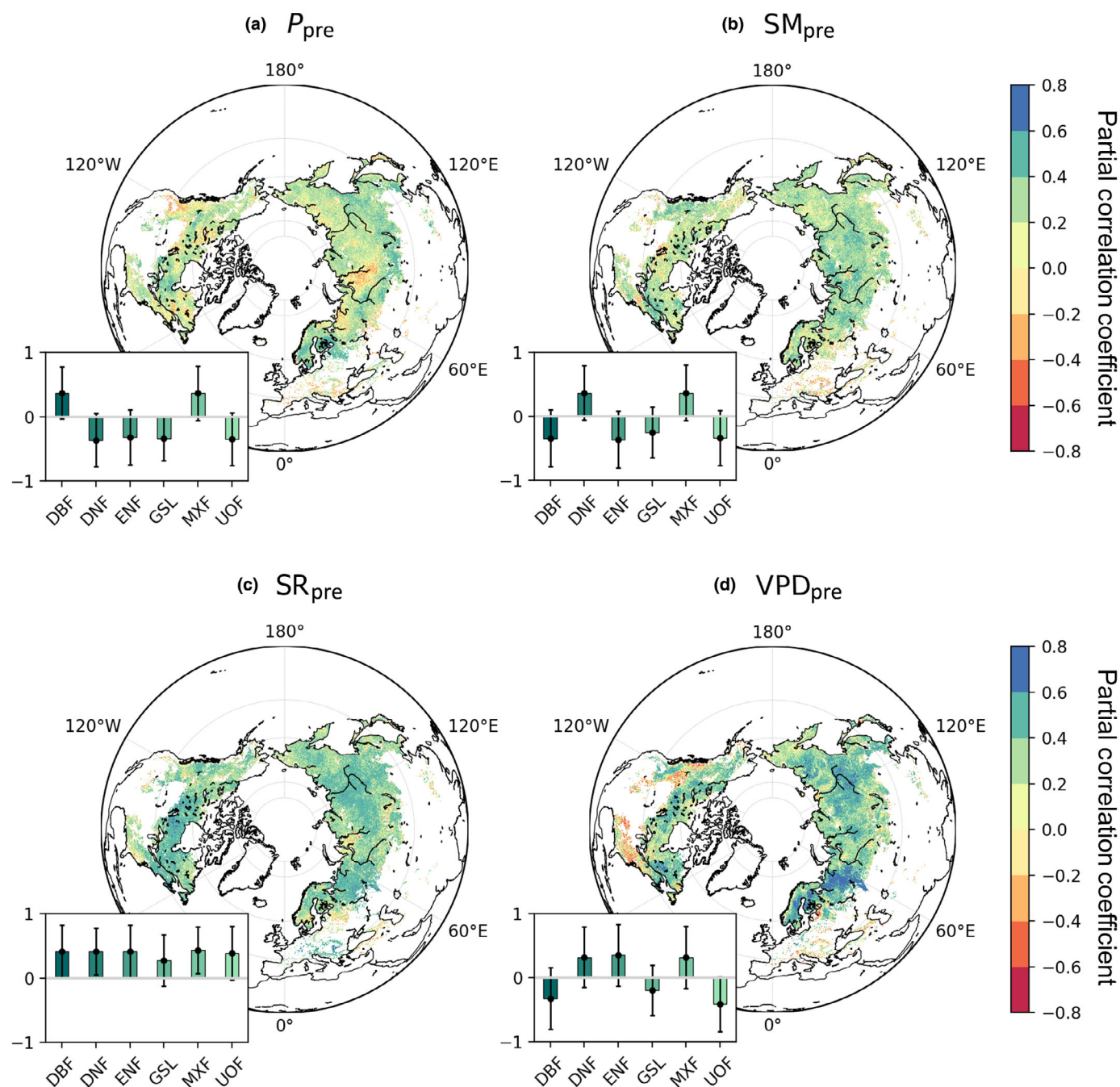


Fig. 3 The spatial pattern of partial dependency of model residuals with four environmental variables of pre-season precipitation (P_{pre} ; a), soil moisture (SM_{pre} ; b), solar radiation (SR_{pre} ; c), and vapor pressure deficit (VPD_{pre} ; d). The inserted figures show the partial correlation coefficients across plant functional types (PFTs), with error bars indicating the standard deviation (SD). DBF, deciduous broadleaf forest; DNF, deciduous needleleaf forest; ENF, evergreen needleleaf forest; GSL, grass/shrubland; MXF, mixed forest; UOF, unknown/other forest.

ENF, fell in between. An additional analysis focusing on the LUD maps predicted by the revised models for the four selected years (Fig. 6d–g for OPT-S; Fig. 6h–k for OPT-VPD; Fig. 1g–j for satellite-derived benchmark) revealed that the revised models effectively captured the satellite-derived phenology pattern both spatially and temporally. This observation further supports the improved accuracy of the revised models in predicting spring phenology across the Northern Hemisphere.

We next examined the model residuals of the revised models and their associations with other environmental variables that were not represented in the default OPT model (Fig. 7). Our results revealed that the default OPT model had the highest absolute value of the model residuals' partial correlation coefficient, consistently across all PFTs and environmental variables examined. As expected, the revised OPT-S model significantly reduced the magnitude of the model residuals' partial correlation value

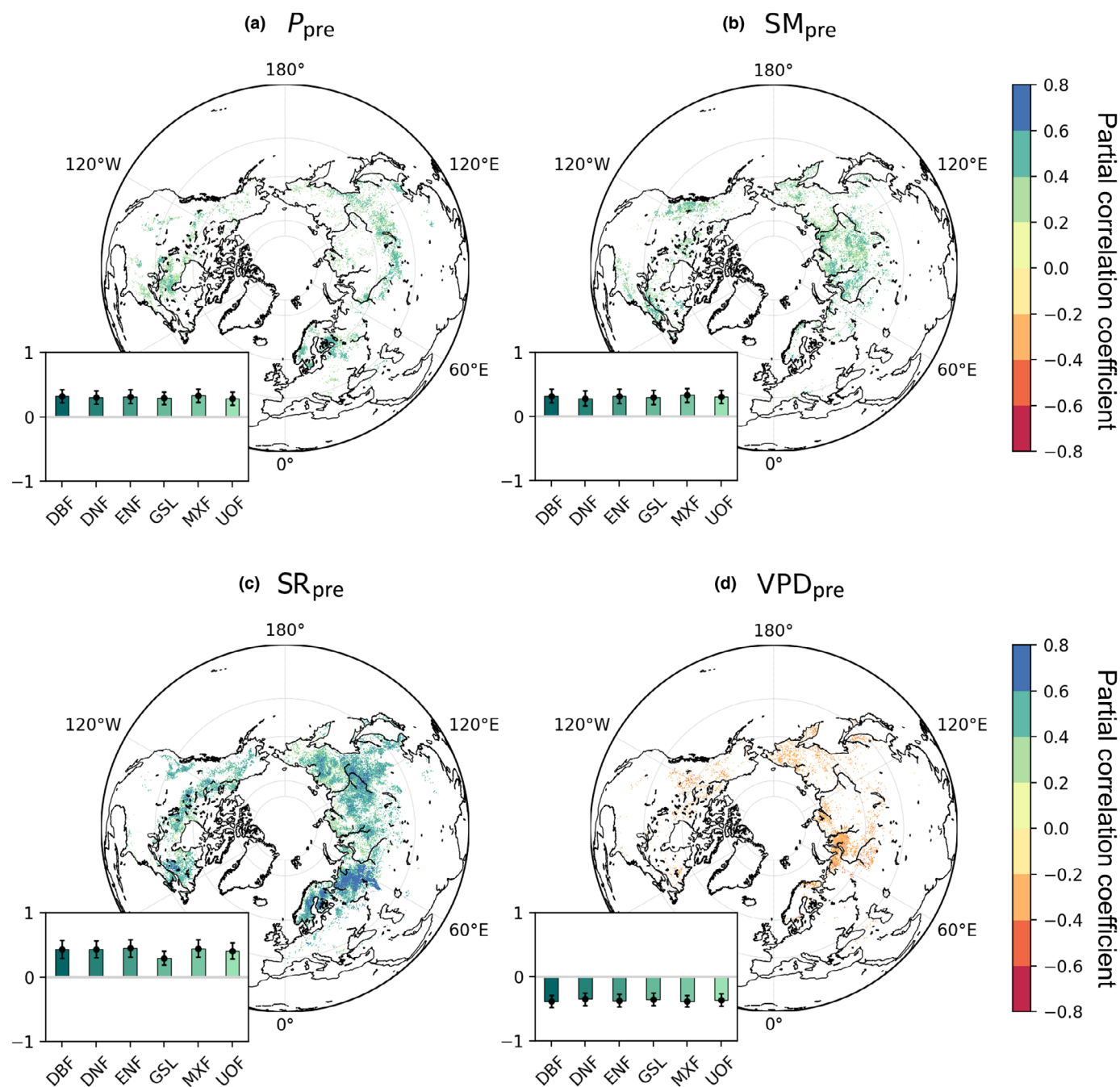


Fig. 4 The spatial pattern of partial dependency of model residuals with four dominant environmental variables of pre-season precipitation (P_{pre} ; a), soil moisture (SM_{pre} ; b), solar radiation (SR_{pre} ; c), and vapor pressure deficit (VPD_{pre} ; d) after adding the ecological constraint and excluding other environmental variables' effects (see the [Materials and Methods](#) section). The inserted figures show the partial correlation coefficients across plant functional types (PFTs), with error bars indicating the standard deviation (SD). DBF, deciduous broadleaf forest; DNF, deciduous needleleaf forest; ENF, evergreen needleleaf forest; GSL, grass/shrubland; MXF, mixed forest; UOF, unknown/other forest.

for SR_{pre} (e.g. from a value of *c.* 0.39 in the default OPT to a value of *c.* 0.21 in the OPT-S model) consistently across all PFTs examined. Surprisingly, it also reduced the partial correlation coefficient magnitude slightly for P_{pre} (except for GSL), SM_{pre} (except for MXF), and VPD_{pre} (except for MXF). Similar findings were observed for OPT-VPD, which not only led to a significant reduction in the model residuals' partial correlation

coefficient magnitude for VPD_{pre} as expected but also caused some reduction in the partial correlation coefficient magnitude for P_{pre} , SM_{pre} , and SR_{pre} . These findings collectively reveal that the revised OPT models are effective, as they not only improve the model performance (as shown in Fig. 6) by reducing the model residuals' partial correlation coefficient magnitude for SR_{pre} and/or VPD_{pre} , but they also do not provoke a rise in the

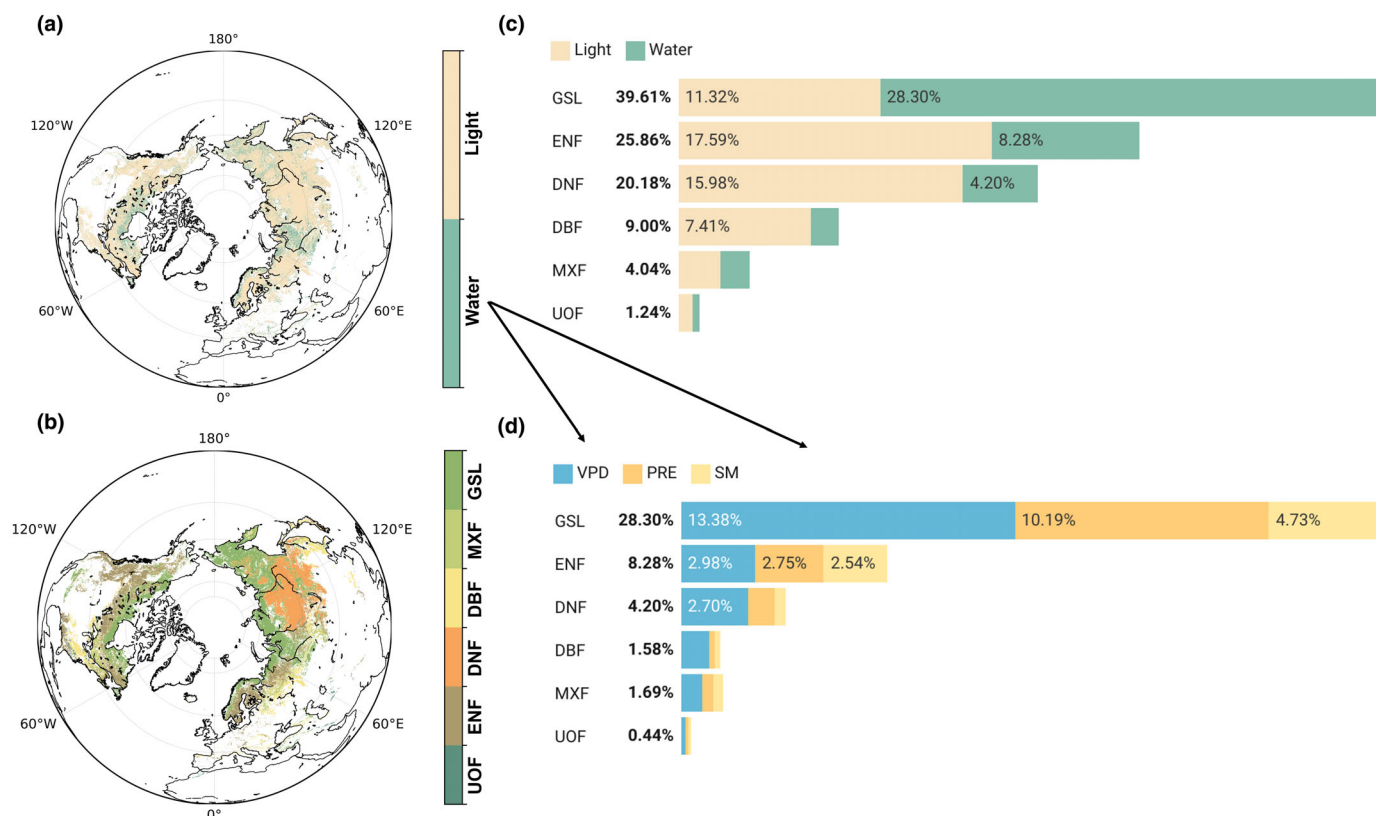


Fig. 5 Statistical analysis across different plant functional types (PFTs). Spatial pattern of the dominant influential factors of light or water stress factors on optimality (OPT) model residual (a). Notably, if the maximum absolute correlation was from solar radiation (SR), the attributed factor was light; otherwise, precipitation (P), soil moisture (SM), and vapor pressure deficit (VPD) were all attributed to water. (b) The land cover type from the HILDA+ product, (c) the percentage of light and water limitation across different PFTs, whereas (d) shows the quantitative water stress composition of VPD, P, and SM across different PFTs. DBF, deciduous broadleaf forest; DNF, deciduous needleleaf forest; ENF, evergreen needleleaf forest; GSL, grass/shrubland; MXF, mixed forest; UOF, unknown/other forest.

model residuals' partial correlation coefficient magnitude for other environmental variables not included in the models (e.g. P_{pre} and SM_{pre}).

Discussion

This study presents three key findings. First, we discover that the default OPT model (relying on temperature and photoperiod as input) can effectively characterize intrasite spring phenology variability over the past three decades in the Northern Hemisphere. However, significant model residuals indicate that the current OPT model does not capture certain underlying mechanisms regulating spring phenology. Second, by attributing model residuals to several candidate causes (i.e. H1-landscape PFT heterogeneity, H2-climate anomaly, and H3-other environmental cues not represented in the current OPT model), our results reject the first two hypotheses. Instead, we find that considerable model residuals are associated with light and water stress factors, which significantly constrain intrasite decadal spring phenology variability. Last, our improved OPT-S model, by incorporating light, or OPT-VPD model, by incorporating water stress factors, reveals substantial model performance improvement without

having an influence on the partial correlation of model residuals with other environmental variables. This suggests the effectiveness of model improvements and potential mechanisms underlying this model representation. These findings altogether highlight the significant role of SR and water stress factors in influencing intrasite decadal spring phenology variability. They also suggest ways to enhance our understanding and modeling of spring phenology responses to climate change, providing critical insights into various phenology-related ecological processes and ecosystem consequences.

Consistent with several recent studies conducted using site-species phenology records (Flynn & Wolkovich, 2018; Meng *et al.*, 2021) and site-scale long-term satellite-derived phenology records (Moon *et al.*, 2021; Gu *et al.*, 2023), our research demonstrates that the OPT-based prognostic phenology model (Meng *et al.*, 2021) effectively characterizes intrasite spring phenology variability, with a mean correlation coefficient of 0.71 and a mean RMSE of 7.08 d. This finding suggests that the mechanistic understanding and modeling developed over the years can be applied to even larger scales across the entire Northern Hemisphere. However, despite this agreement, we also observed significant model residuals (defined as modeled LUD

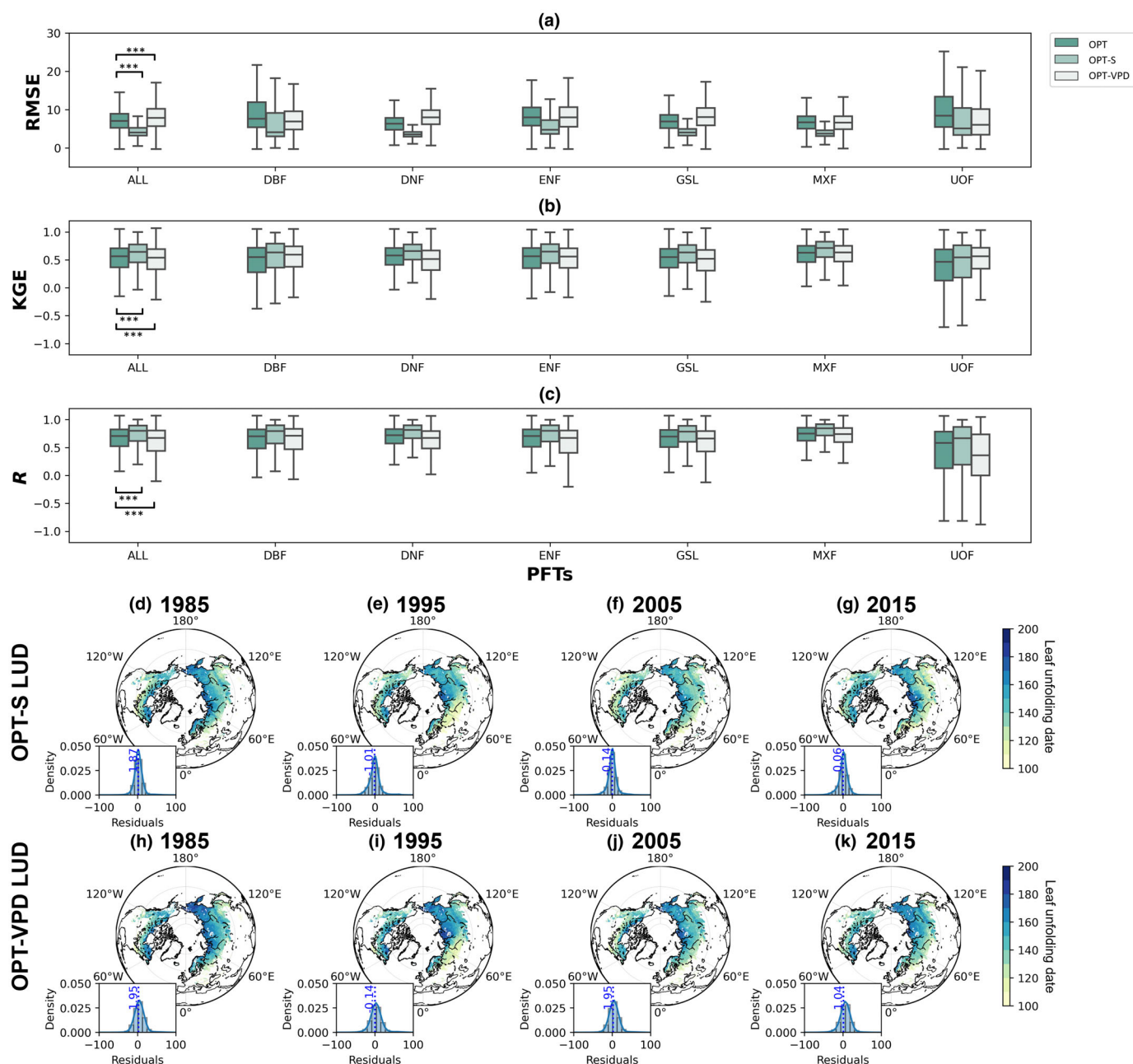


Fig. 6 The performance of the improved optimality (OPT)-S, OPT-VPD compared with the origin OPT in modeling plant spring phenology across PFTs, using the three accuracy metrics of RMSE (a), KGE (b), R (c), where ‘***’ indicates that there existed a significant difference between different groups (P -value < 0.001) and the box spans from the first quartile (Q1) to the third quartile (Q3), with a line marking the median and the whiskers extend to the farthest data point within 1.5 times the interquartile range (IQR) from the box. Spatial and temporal patterns of the OPT-S and OPT-VPD model result in (d–k) compared with the start of season date derived from the Global Inventory Modeling and Mapping Studies (GIMMS) NDVI3g dataset Fig. 1(g–j) in the selected years: 1985, 1995, 2005, and 2015, where the blue dashed line shows the mean value of the histogram. ALL, all the plant functional types; DBF, deciduous broadleaf forest; DNF, deciduous needleleaf forest; ENF, evergreen needleleaf forest; GSL, grass/shrubland; MXF, mixed forest; UOF, unknown/other forest; RMSE, root mean square error; KGE, Kling–Gupta efficiency; R , Pearson’s correlation coefficients; PFTs, plant functional types; LUD, lead unfolding date; VPD, vapor pressure deficit.

minus satellite-derived LUD) across all PFTs in the Northern Hemisphere, with 62.03% of the study areas holding an RMSE value ranging from 5 to 10 d (Fig. 2). This uncertainty is not negligible, given that the mean phenology change over the past three decades in the same area is *c.* 5–10 d (Meng *et al.*, 2021; Zhao *et al.*, 2021). This indicates that there is room for improvement

in the current OPT model’s representation of spring phenology mechanisms.

To examine the potential causes of the considerable model residuals underlying the default OPT model, we considered three candidate hypotheses: H1 – landscape PFT heterogeneity (due to our analysis being conducted at a coarse spatial resolution of

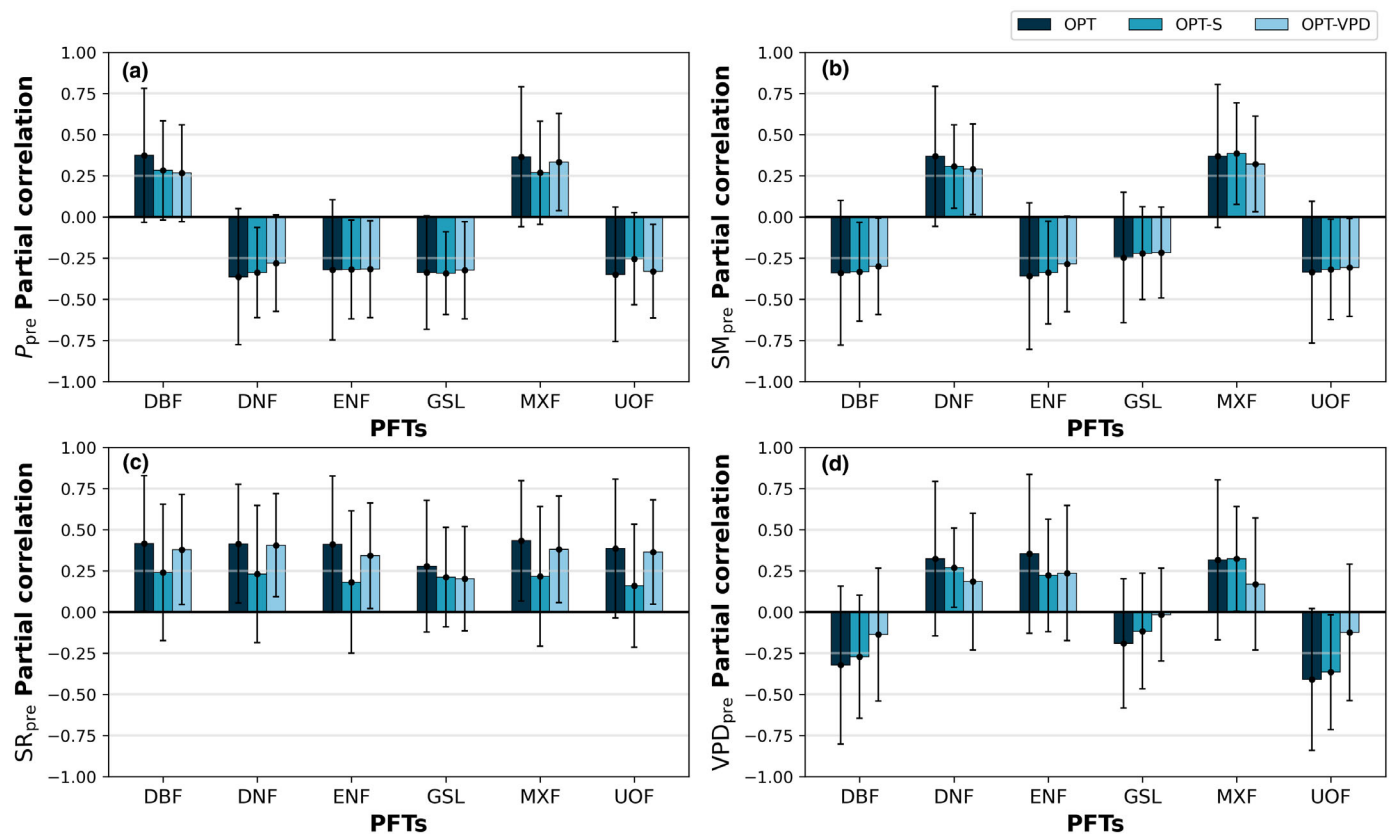


Fig. 7 The partial dependency residuals from three models (optimality (OPT), OPT-S, and OPT-VPD) with four environmental variables of pre-season precipitation (P_{pre} ; a), pre-season soil moisture (SM_{pre} ; b), pre-season solar radiation (SR_{pre} ; c), and pre-season vapor pressure deficit (VPD_{pre} ; d), with error bars indicating the standard deviation. PFTs, plant functional types; DBF, deciduous broadleaf forest; DNF, deciduous needleleaf forest; ENF, evergreen needleleaf forest; GSL, grass/shrubland; MXF, mixed forest; UOF, unknown/other forest.

1/12°, with one pixel often containing multiple PFTs; Pan *et al.*, 2023); H2 – climate anomaly (assuming the OPT model can track intrasite spring phenology variability in normal years but exhibits significant biases in years with extreme cold or hot conditions; Liu & Zhang, 2020); and H3 – other environmental cues underrepresented in the current OPT model (as observed and hypothesized in Gu *et al.*, 2023). Our analysis rejects the first two hypotheses (Fig. S3), suggesting that spatial PFT heterogeneity has a limited influence on decadal OPT spring phenology modeling, and the OPT model is (near)-equally skilled in characterizing spring phenology variability in both normal and extreme climate conditions. This finding is in line with previous findings (Meng *et al.*, 2021; Kim *et al.*, 2022; Gu *et al.*, 2023). The OPT model's effectiveness is likely due to its ability to account for the concurrent association between endodormancy and ecodormancy phases, accurately representing the interdependent connection between plant survival in inhospitable cold conditions (or endodormancy, as demonstrated by the chilling influence) and the role of the surrounding environment in prompting the transition from the endodormancy stage to the active development phase (evidenced by the combined impact of forcing and photoperiod).

We then examined H3 and discovered that environmental constraints related to light and water stress significantly regulate

intrasite spring phenology variability, as evidenced by the substantial partial correlation between model residuals and these variables (Fig. 7), supporting H3. This finding aligns with Gu *et al.* (2023), which examined hundreds of temperate ecosystem sites across the northern and eastern regions of the United States and several recent empirical studies (Garonna *et al.*, 2018; Peau-celle *et al.*, 2019) that observed the significant influence of light or water cues on regulating intra-site spring phenology variability. Collectively, these studies suggest that environmental factors beyond those explicitly represented in the current OPT model (i.e. temperature and photoperiod) should also be considered when interpreting and modeling large-scale spring phenology variability, such as across the entire Northern Hemisphere examined in this study.

Despite the general agreement with Gu *et al.* (2023), we also observed some significant differences. Specifically, the dominant model residual's partial correlation with the examined environmental variables varies considerably across different PFTs (Fig. 7). Grass/shrubland ecosystems are primarily dominated by water-stress-related factors, while other PFTs (mainly forest-related ecosystems) are dominated by SR. Interestingly, this observation is consistent with several site-/regional-level empirical studies (Felton *et al.*, 2020; Legesse *et al.*, 2021; Ren

et al., 2022a) that also observed varying dominant environmental cues for spring phenology across PFTs, with grassland ecosystem phenology tending to be more strongly regulated by water stress factors, such as snow and rainfall. The underlying mechanism for this observation could be that grassland ecosystems typically inhabit mesic environments with limited water supply and shallow rooting depths, which restrict their access to deep soil water (Shen *et al.*, 2011; Fu *et al.*, 2021; Ren *et al.*, 2022a). Consequently, water stress often outweighs other factors in constraining earlier spring phenology variability. By contrast, high-biomass ecosystems (like forests) usually have greater soil water storage and deeper root systems, allowing them to access deep soil water. Thus, water stress factors have a reduced impact on regulating spring phenology and light becomes the predominant factor (Shen *et al.*, 2011; Fu *et al.*, 2021; Ren *et al.*, 2022a).

The revised OPT-S and OPT-VPD models demonstrated substantial improvements over the original OPT model, significantly reducing the partial dependency of model residuals on SR_{pre} and VPD_{pre} without increasing dependency on other excluded environmental factors. The enhanced model performance of these models – achieved by replacing photoperiod in the default OPT model with SR or VPD – likely stems from the fact that SR serves as a more dynamic and responsive indicator of intrasite decadal spring phenology variability compared to photoperiod, which is static and determined solely by geographic location and calendar date. Unlike photoperiod, SR is influenced by a range of external factors, such as topography, and is highly sensitive to early-season weather variability, including fluctuations in cloud cover, rainfall, and snowfall, all of which could play roles in regulating plant spring phenology (Zeng *et al.*, 2010; Jin *et al.*, 2017; Flynn & Wolkovich, 2018; Wang *et al.*, 2020a; Ettinger *et al.*, 2021; Ren *et al.*, 2022b). Notably, we rigorously tested this hypothesis in a previous paper (Gu *et al.*, 2023) that focused on temperate forests in the Eastern United States. Here we extended a similar analysis to the entire Northern Hemisphere, and we found that the same pattern holds, suggesting our earlier findings are scalable to broader contexts. Similarly, VPD is a more dynamic variable than photoperiod, related to early-season plant growth environmental conditions of light and water availability as well as sky/weather conditions. This makes VPD a more information-rich variable than photoperiod. For example, high VPD can lead to increased evapotranspiration, resulting in increased water stress conditions in the plant canopy (Guerrieri *et al.*, 2016; Grossiord *et al.*, 2020). This water stress can disrupt the plants' ability to perceive and respond to environmental cues such as SR, affecting essential processes like photosynthesis and growth, thereby functioning as another crucial environmental cue for spring phenology (Du *et al.*, 2020; Ganjurjav *et al.*, 2020; Peng *et al.*, 2021).

Additionally, the significant model performance improvement observed in the revised OPT models incorporating SR or VPD could be attributed to these variables being better metrics than photoperiod for approximating and modeling early-season plant photosynthesis potential. In recent years, there has been an increasing consensus suggesting that plant spring phenology can be viewed as an eco-evolutionary adaptive strategy aimed at maximizing photosynthetic carbon gain while minimizing the

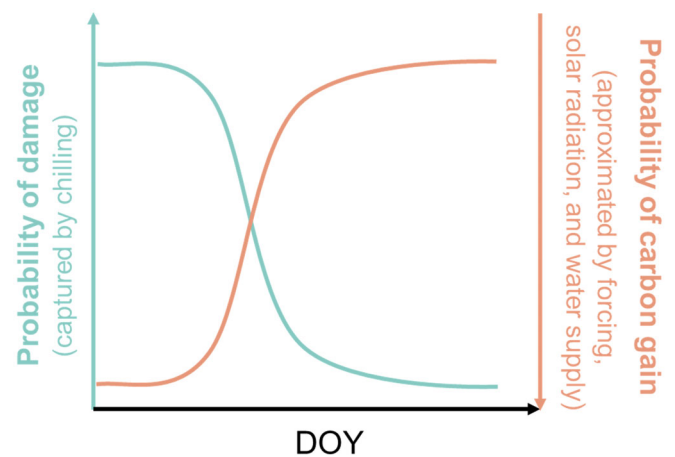


Fig. 8 A hypothesis framework indicating spring phenology as an optimal strategy for plants to minimize frost damage risk (captured by chilling) while maximizing photosynthetic carbon gain (approximated by forcing, solar radiation, and water supply). DOY, day of year.

potential risk of frost damage (Forrest & Miller-Rushing, 2010; Anderson *et al.*, 2012; Hendry, 2016). Models incorporating this strategy have been shown to outperform conventional models (e.g. GDDs and sequential models) (Meng *et al.*, 2021; Gu *et al.*, 2023). Building upon this eco-evolutionary OPT theory, our study not only demonstrates the effectiveness of using this theoretical framework for improved modeling of spring phenology in the Northern Hemisphere ecosystems but also highlights that SR (and VPD) are substantially better metrics for approximating and modeling early-season plant photosynthesis potential (Fig. 8). This discovery is also consistent with basic plant ecophysiology theory (e.g. the Farquhar-type biochemical photosynthesis modeling principle – Farquhar *et al.* 1980; and the stomatal regulation principle – Medlyn *et al.*, 2011), which suggests that both SR and VPD play important roles in regulating plant photosynthesis activities. This is because photosynthetic carbon gain is more correlated with SR than photoperiod given its direct constraint on plant photosynthesis rates (Durand *et al.*, 2021), while VPD information enriches the water stress effects on plant spring phenology (Pegoraro *et al.*, 2007; Grossiord *et al.*, 2020). The dominant role of VPD and SR in regulating early-season plant photosynthesis potential has also been observed to vary with PFT and plant growth conditions (Descals *et al.*, 2023), supporting our observations as observed in Figs 5 and 6. Despite this, future studies should seek more direct observational and experimental evidence to confirm the above reasoning.

Our research highlights two crucial avenues for advancing future phenology investigations. First, the considerable variation in model performance across different PFTs suggests that the phenological responses to environmental cues might differ among different PFTs, indicating that a one-size-fits-all model might not be the best approach for predicting spring phenology (Richardson *et al.*, 2018a; Ji *et al.*, 2021). Future studies should consider developing and testing PFT-specific models, as this approach will enable explicit representations of the diverse

phenological responses observed among distinct PFTs (Zhao *et al.*, 2021). Second, our findings highlight a strong need to include and better represent SR and VPD in spring phenology modeling. For example, in the terrestrial biosphere modeling community, the process-based photosynthesis modeling framework (e.g. integrating Farquhar-type photosynthesis with Medlyn-type stomatal conductance models; Guo *et al.*, 2022) has been increasingly favored in recent years and could be adapted for our case to better approximate early-season plant photosynthesis potential, thereby improving the testing of our theoretical framework as presented in Fig. 8. Several advantages could be offered if a more mechanistic photosynthesis modeling framework is considered, including but not limited to (1) providing more direct evidence to evaluate the proposed framework in Fig. 8, (2) considering more environmental variables including those metrics of water stresses, (3) conducting diagnostic analysis to better understand key environmental variables responsible for spring phenology across landscapes and geographical extents, and (4) improving the assessment of future climate change impacts on spring phenology dynamics. Similarly, experimental-based evidence or long-term ground observational datasets are needed to help reveal the fundamental mechanisms underlying spring phenology regulation, providing strong theoretical support to further test the framework we proposed in this study.

Conclusion

The shift in spring phenology due to climate change has already generated impacts on large-scale biogeochemical cycles and many essential ecosystem processes. This has prompted the development of numerous prognostic models in recent decades, with the OPT strategy model gaining increasing attention. However, a thorough examination of the OPT model on a regional level, considering environmental factors beyond just temperature and photoperiod as currently captured by existing models, remains insufficient. In this study, we evaluated the current ability of the OPT model to characterize the decadal intra-site variability of spring phenology in the Northern Hemisphere and found that it reasonably captured the spatial and temporal patterns of spring phenology variability in the region; however, considerable model residuals remain. A significant correlation was found between model residuals and SR_{pre} as well as VPD_{pre} , highlighting their importance in regulating temperate ecosystem phenology. By incorporating these factors, the revised models (OPT-S, OPT-VPD) demonstrated greater model performance and minimal impact on the partial dependency of the model residuals on other unused environmental variables, highlighting the effectiveness of these revised models. These results contribute to an enhanced understanding and model representation of large-scale spring phenology variability across the Northern Hemisphere under recent climate change. This improved understanding and the revised models have the potential to be used for simulating the impacts of continued climate change on spring phenology as well as its impacts on many other essential ecological processes.

Acknowledgements

This work was supported by the National Natural Science Foundation of China (grant no. 31922090) and the Hong Kong Research Grant Council General Research Fund (grant no. 17305321). JW was supported by the Hong Kong Research Grant Council Collaborative Research Fund (grant no. C5062-21GF), the HKU Seed Funding for Strategic Interdisciplinary Research Scheme, the HKU Science Faculty RAE Improvement Fund 2023–24, and the Innovation and Technology Fund (funding support to State Key Laboratories of Agrobiotechnology). MD was supported by the Carbon Mitigation Initiative of Princeton University and the NSF (grant no. 2017804).





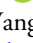



Competing interests

None declared.

Author contributions

YG and JW conceived the study. YG performed the analyses. YG, LM, YW, ZW, YP, YZ, MD and JW contributed to interpreting the results. YG drafted the manuscript with constructive input from JW. YG, LM, YW, ZW, YP, YZ, MD and JW contributed to the manuscript editing.

ORCID

Matteo Detto  <https://orcid.org/0000-0003-0494-188X>
 Yating Gu  <https://orcid.org/0000-0001-8312-2473>
 Lin Meng  <https://orcid.org/0000-0002-1603-4200>
 Yuhao Pan  <https://orcid.org/0000-0002-5384-4624>
 Yantian Wang  <https://orcid.org/0000-0003-2686-5275>
 Jin Wu  <https://orcid.org/0000-0001-8991-3970>
 Zherong Wu  <https://orcid.org/0000-0002-9536-1348>
 Yingyi Zhao  <https://orcid.org/0009-0001-5392-3402>

Data availability

GIMMS NDVI3g dataset is available at <https://data.tpdc.ac.cn/en/data/9775f2b4-7370-4e5e-a537-3482c9a83d88/>, TerraClimate dataset is available at <https://www.climatologylab.org/terraclimate.html>, CRU_TS v4.03 dataset is available at <https://crudata.uea.ac.uk/cru/data/hrg/>, and GLDAS dataset is available at <https://ldas.gsfc.nasa.gov/gldas>.

References

- Abatzoglou JT, Dobrowski SZ, Parks SA, Hegewisch KC. 2018. TerraClimate, a high-resolution global dataset of monthly climate and climatic water balance from 1958–2015. *Scientific Data* 5: 1–12.
- Adams BT, Matthews SN, Iverson LR, Prasad AM, Peters MP, Zhao K. 2021. Spring phenological variability promoted by topography and vegetation assembly processes in a temperate forest landscape. *Agricultural and Forest Meteorology* 308–309: 108578.
- Anderson JT, Inouye DW, McKinney AM, Colautti RI, Mitchell-Olds T. 2012. Phenotypic plasticity and adaptive evolution contribute to advancing flowering

- phenology in response to climate change. *Proceedings of the Royal Society B: Biological Sciences* 279: 3843–3852.
- Badeck F-W, Bondeau A, Böttcher K, Doktor D, Lucht W, Schaber J, Sitch S. 2004. Responses of spring phenology to climate change. *New Phytologist* 162: 295–309.
- Beck HE, Zimmermann NE, McVicar TR, Vergopolan N, Berg A, Wood EF. 2018. Present and future Köppen–Geiger climate classification maps at 1-km resolution. *Scientific Data* 5: 1–12.
- Buermann W, Forkel M, O'sullivan M, Sitch S, Friedlingstein P, Haverd V, Jain AK, Kato E, Kautz M, Lienert S. 2018. Widespread seasonal compensation effects of spring warming on northern plant productivity. *Nature* 562: 110–114.
- Caldararu S, Purves DW, Smith MJ. 2016. The effect of using the plant functional type paradigm on a data-constrained global phenology model. *Biogeosciences* 13: 925–941.
- Chamberlain CJ, Wolkovich EM. 2021. Late spring freezes coupled with warming winters alter temperate tree phenology and growth. *New Phytologist* 231: 987–995.
- Chuine I, Cambron G, Comtois P. 2000. Scaling phenology from the local to the regional level: advances from species-specific phenological models. *Global Change Biology* 6: 943–952.
- Chuine I, Cortazar-Atauri IGd, Kramer K, Hänninen H. 2013. Plant development models. In: *Phenology: an integrative environmental science*. New York, NY, USA: Springer, 275–293.
- Cohen EB, Satterfield DA. 2020. 'Chancing on a spectacle': co-occurring animal migrations and interspecific interactions. *Ecography* 43: 1657–1671.
- Descals A, Verger A, Yin G, Filella I, Fu YH, Piao S, Janssens IA, Peñuelas J. 2023. Radiation-constrained boundaries cause nonuniform responses of the carbon uptake phenology to climatic warming in the Northern Hemisphere. *Global Change Biology* 29: 719–730.
- Du J, Li K, He Z, Chen L, Lin P, Zhu X. 2020. Daily minimum temperature and precipitation control on spring phenology in arid-mountain ecosystems in China. *International Journal of Climatology* 40: 2568–2579.
- Durand M, Murchie EH, Lindfors AV, Urban O, Aphalo PJ, Robson TM. 2021. Diffuse solar radiation and canopy photosynthesis in a changing environment. *Agricultural and Forest Meteorology* 311: 108684.
- Ettinger A, Buonaiuto D, Chamberlain C, Morales-Castilla I, Wolkovich E. 2021. Spatial and temporal shifts in photoperiod with climate change. *New Phytologist* 230: 462–474.
- Fang J, Lutz JA, Wang L, Shugart HH, Yan X. 2020. Using climate-driven leaf phenology and growth to improve predictions of gross primary productivity in North American forests. *Global Change Biology* 26: 6974–6988.
- Farquhar GD, von Caemmerer S, Berry JA. 1980. A biochemical model of photosynthetic CO₂ assimilation in leaves of C₃ species. *Planta* 149: 78–90.
- Felton AJ, Slette IJ, Smith MD, Knapp AK. 2020. Precipitation amount and event size interact to reduce ecosystem functioning during dry years in a mesic grassland. *Global Change Biology* 26: 658–668.
- Flynn D, Wolkovich E. 2018. Temperature and photoperiod drive spring phenology across all species in a temperate forest community. *New Phytologist* 219: 1353–1362.
- Forrest J, Miller-Rushing AJ. 2010. Toward a synthetic understanding of the role of phenology in ecology and evolution. *Philosophical Transactions of the Royal Society of London. Series B, Biological Sciences* 365: 1555.
- Friedl M, Gray J, Sulla-Menashe D. 2019. MCD12Q2 MODIS/Terra+ Aqua Land Cover Dynamics Yearly L3 Global 500m SIN Grid V006. NASA EOSDIS Land Processes DAAC.
- Fu Y, Li X, Zhou X, Geng X, Guo Y, Zhang Y. 2020. Progress in plant phenology modeling under global climate change. *Science China Earth Sciences* 63: 1237–1247.
- Fu YH, Zhou X, Li X, Zhang Y, Geng X, Hao F, Zhang X, Hanninen H, Guo Y, De Boeck HJ. 2021. Decreasing control of precipitation on grassland spring phenology in temperate China. *Global Ecology and Biogeography* 30: 490–499.
- Ganjurjav H, Gornish ES, Hu G, Schwartz MW, Wan Y, Li Y, Gao Q. 2020. Warming and precipitation addition interact to affect plant spring phenology in alpine meadows on the central Qinghai-Tibetan Plateau. *Agricultural and Forest Meteorology* 287: 107943.
- Garonna I, de Jong R, Stöckli R, Schmid B, Schenkel D, Schimel D, Schaepman ME. 2018. Shifting relative importance of climatic constraints on land surface phenology. *Environmental Research Letters* 13: 24025.
- Geng X, Fu YH, Hao F, Zhou X, Zhang X, Yin G, Vitasse Y, Piao S, Niu K, De Boeck HJ *et al.* 2020. Climate warming increases spring phenological differences among temperate trees. *Global Change Biology* 26: 5979–5987.
- Gerst KL, Crimmins TM, Posthumus EE, Rosemartin AH, Schwartz MD. 2020. How well do the spring indices predict phenological activity across plant species? *International Journal of Biometeorology* 64: 889–901.
- Gonsamo A, Chen JM, Price DT, Kurz WA, Wu C. 2012. Land surface phenology from optical satellite measurement and CO₂ eddy covariance technique. *Journal of Geophysical Research: Biogeosciences* 117. doi: 10.1029/2012jg002070.
- Grossiord C, Buckley TN, Cernusak LA, Novick KA, Poulter B, Siegwolf RTW, Sperry JS, McDowell NG. 2020. Plant responses to rising vapor pressure deficit. *New Phytologist* 226: 1550–1566.
- Gu Y, Zhao Y, Guo Z, Meng L, Zhang K, Wang J, Lee CKF, Xie J, Wang Y, Yan Z *et al.* 2023. The underappreciated importance of solar radiation in constraining spring phenology of temperate ecosystems in the Northern and Eastern United States. *Remote Sensing of Environment* 294: 113617.
- Guerrieri R, Lepine L, Asbjornsen H, Xiao J, Ollinger SV. 2016. Evapotranspiration and water use efficiency in relation to climate and canopy nitrogen in US forests. *Journal of Geophysical Research: Biogeosciences* 121: 2610–2629.
- Guo Z, Yan Z, Majcher BM, Lee CK, Zhao Y, Song G, Wang B, Wang X, Deng Y, Michaletz ST. 2022. Dynamic biotic controls of leaf thermoregulation across the diel timescale. *Agricultural and Forest Meteorology* 315: 108827.
- Gupta HV, Kling H, Yilmaz KK, Martinez GF. 2009. Decomposition of the mean squared error and NSE performance criteria: implications for improving hydrological modelling. *Journal of Hydrology* 377: 80–91.
- Harris I, Osborn TJ, Jones P, Lister D. 2020. Version 4 of the CRU TS monthly high-resolution gridded multivariate climate dataset. *Scientific Data* 7: 109.
- Heide O. 2003. High autumn temperature delays spring bud burst in boreal trees, counterbalancing the effect of climatic warming. *Tree Physiology* 23: 931–936.
- Hendry AP. 2016. Key questions on the role of phenotypic plasticity in eco-evolutionary dynamics. *Journal of Heredity* 107: 25–41.
- Hmimina G, Dufrêne E, Pontailier J-Y, Delpierre N, Aubinet M, Caquet B, De Grandcourt A, Burban B, Flechard C, Granier A. 2013. Evaluation of the potential of MODIS satellite data to predict vegetation phenology in different biomes: an investigation using ground-based NDVI measurements. *Remote Sensing of Environment* 132: 145–158.
- Huang J-G, Zhang Y, Wang M, Yu X, Deslauriers A, Fonti P, Liang E, Mäkinen H, Oberhuber W, Rathgeber CBK *et al.* 2023. A critical thermal transition driving spring phenology of Northern Hemisphere conifers. *Global Change Biology* 29: 1606–1617.
- Ji S, Ren S, Li Y, Dong J, Wang L, Quan Q, Liu J. 2021. Diverse responses of spring phenology to pre-season drought and warming under different biomes in the North China Plain. *Science of the Total Environment* 766: 144437.
- Jin H, Jönsson AM, Bolmgren K, Langvall O, Eklundh L. 2017. Disentangling remotely-sensed plant phenology and snow seasonality at northern Europe using MODIS and the plant phenology index. *Remote Sensing of Environment* 198: 203–212.
- Kim S, Kim TK, Yoon S, Jang K, Chun J-H, Won M, Lim J-H, Kim HS. 2022. Quantifying the importance of day length in process-based models for the prediction of temperate spring flowering phenology. *Science of the Total Environment* 843: 156780.
- Legesse TG, Dong G, Jiang S, Chen J, Dong X, Daba NA, Sorecha EM, Qu L, Tian L, Shao C. 2021. Small precipitation events enhance the Eurasian grassland carbon sink. *Ecological Indicators* 131: 108242.
- Li X, Fu YH, Chen S, Xiao J, Yin G, Li X, Zhang X, Geng X, Wu Z, Zhou X. 2021. Increasing importance of precipitation in spring phenology with decreasing latitudes in subtropical forest area in China. *Agricultural and Forest Meteorology* 304: 108427.
- Li Y, Zhang W, Schwalm CR, Gentile P, Smith WK, Ciaia P, Kimball JS, Gazol A, Kannenberg SA, Chen A *et al.* 2023. Widespread spring phenology

- effects on drought recovery of Northern Hemisphere ecosystems. *Nature Climate Change* 13: 182–188.
- Lian X, Piao S, Li LZ, Li Y, Huntingford C, Ciais P, Cescatti A, Janssens IA, Peñuelas J, Buermann W. 2020. Summer soil drying exacerbated by earlier spring greening of northern vegetation. *Science Advances* 6: eaax0255.
- Liu D. 2020. A rational performance criterion for hydrological model. *Journal of Hydrology* 590: 125488.
- Liu L, Cao R, Shen M, Chen J, Wang J, Zhang X. 2019. How does scale effect influence spring vegetation phenology estimated from satellite-derived vegetation indexes? *Remote Sensing* 11: 2137.
- Liu L, Zhang X. 2020. Effects of temperature variability and extremes on spring phenology across the contiguous United States from 1982 to 2016. *Scientific Reports* 10: 17952.
- Liu Q, Fu YH, Zhu Z, Liu Y, Liu Z, Huang M, Janssens IA, Piao S. 2016. Delayed autumn phenology in the Northern Hemisphere is related to change in both climate and spring phenology. *Global Change Biology* 22: 3702–3711.
- Liu Y, Wu C, Wang X, Zhang Y. 2023. Contrasting responses of peak vegetation growth to asymmetric warming: evidences from FLUXNET and satellite observations. *Global Change Biology* 29: 2363–2379.
- Ma R, Shen X, Zhang J, Xia C, Liu Y, Wu L, Wang Y, Jiang M, Lu X. 2022. Variation of vegetation autumn phenology and its climatic drivers in temperate grasslands of China. *International Journal of Applied Earth Observation and Geoinformation* 114: 103064.
- McMaster GS, Wilhelm W. 1997. Growing degree-days: one equation, two interpretations. *Agricultural and Forest Meteorology* 87: 291–300.
- Medlyn BE, Duursma RA, Eamus D, Ellsworth DS, Prentice IC, Barton CVM, Crous KY, De Angelis P, Freeman M, Wingate L. 2011. Reconciling the optimal and empirical approaches to modelling stomatal conductance. *Global Change Biology* 17: 2134–2144.
- Melaas EK, Friedl MA, Richardson AD. 2016. Multiscale modeling of spring phenology across Deciduous Forests in the Eastern United States. *Global Change Biology* 22: 792–805.
- Meng L, Zhou Y, Gu L, Richardson AD, Peñuelas J, Fu Y, Wang Y, Asrar GR, De Boeck HJ, Mao J. 2021. Photoperiod decelerates the advance of spring phenology of six deciduous tree species under climate warming. *Global Change Biology* 27: 2914–2927.
- Moon M, Seyednasrollah B, Richardson AD, Friedl MA. 2021. Using time series of MODIS land surface phenology to model temperature and photoperiod controls on spring greenup in North American deciduous forests. *Remote Sensing of Environment* 260: 112466.
- NASA Global Inventory Modeling and Mapping Studies (GIMMS). 2015. *GIMMS NDVI3g v1 dataset (1981–2015)*. [WWW document] URL <https://ecocast.arc.nasa.gov/data/pub/gimms/3g.v1/>.
- NASA Goddard Earth Sciences Data and Information Services Center. 2023. *Global Land Data Assimilation System (GLDAS)*. Greenbelt, MD, USA: Goddard Earth Sciences Data and Information Services Center (GES DISC).
- Nemani RR. 2003. Climate-driven increases in global terrestrial net primary production from 1982 to 1999. *Science* 300: 1560–1563.
- Nord EA, Lynch JP. 2009. Plant phenology: a critical controller of soil resource acquisition. *Journal of Experimental Botany* 60: 1927–1937.
- Pan Y, Peng D, Chen JM, Myneni RB, Zhang X, Huete AR, Fu YH, Zheng S, Yan K, Yu L. 2023. Climate-driven land surface phenology advance is overestimated due to ignoring land cover changes. *Environmental Research Letters* 18: 44045.
- Park HM. 2009. Comparing group means: *t*-tests and one-way ANOVA using Stata, SAS, R, and SPSS.
- Peaucelle M, Janssens IA, Stocker BD, Descals Ferrando A, Fu YH, Molowny-Horas R, Ciais P, Peñuelas J. 2019. Spatial variance of spring phenology in temperate deciduous forests is constrained by background climatic conditions. *Nature Communications* 10: 5388.
- Pegoraro E, Potosnak MJ, Monson RK, Rey A, Barron-Gafford G, Osmond CB. 2007. The effect of elevated CO₂, soil and atmospheric water deficit and seasonal phenology on leaf and ecosystem isoprene emission. *Functional Plant Biology* 34: 774–784.
- Peng J, Wu C, Zhang X, Ju W, Wang X, Lu L, Liu Y. 2021. Incorporating water availability into autumn phenological model improved China's terrestrial gross primary productivity (GPP) simulation. *Environmental Research Letters* 16: 94012.
- Ren S, Chen X, Pan C. 2022a. Temperature-precipitation background affects spatial heterogeneity of spring phenology responses to climate change in northern grasslands (30°N–55°N). *Agricultural and Forest Meteorology* 315: 108816.
- Ren S, Vitasse Y, Chen X, Peichl M, An S. 2022b. Assessing the relative importance of sunshine, temperature, precipitation, and spring phenology in regulating leaf senescence timing of herbaceous species in China. *Agricultural and Forest Meteorology* 313: 108770.
- Richardson AD, Hufkens K, Milliman T, Aubrecht DM, Chen M, Gray JM, Johnston MR, Keenan TF, Klosterman ST, Kosmala M. 2018a. Tracking vegetation phenology across diverse North American biomes using PhenoCam imagery. *Scientific Data* 5: 1–24.
- Richardson AD, Hufkens K, Milliman T, Aubrecht DM, Furze ME, Seyednasrollah B, Krassovski MB, Latimer JM, Nettles WR, Heiderman RR. 2018b. Ecosystem warming extends vegetation activity but heightens vulnerability to cold temperatures. *Nature* 560: 368–371.
- Richardson AD, Keenan TF, Migliavacca M, Ryu Y, Sonnentag O, Toomey M. 2013. Climate change, phenology, and phenological control of vegetation feedbacks to the climate system. *Agricultural and Forest Meteorology* 169: 156–173.
- Richardson EA, Seeley SD, Walker DR. 1974. A model for estimating the completion of rest for Redhaven and Elberta peach trees. *Journal of the American Society for Horticultural Science* 99: 540–546.
- Schwartz MD, Ahas R, Aasa A. 2006. Onset of spring starting earlier across the Northern Hemisphere. *Global Change Biology* 12: 343–351.
- Shen M, Piao S, Dorji T, Liu Q, Cong N, Chen X, An S, Wang S, Wang T, Zhang G. 2015. Plant phenological responses to climate change on the Tibetan Plateau: research status and challenges. *National Science Review* 2: 454–467.
- Shen M, Tang Y, Chen J, Zhu X, Zheng Y. 2011. Influences of temperature and precipitation before the growing season on spring phenology in grasslands of the central and eastern Qinghai-Tibetan Plateau. *Agricultural and Forest Meteorology* 151: 1711–1722.
- Singh RK, Svystun T, Aldahmash B, Jönsson AM, Bhalariao RP. 2017. Photoperiod and temperature-mediated control of phenology in trees—a molecular perspective. *New Phytologist* 213: 511–524.
- Tao Z, Huang W, Wang H. 2020. Soil moisture outweighs temperature for triggering the green-up date in temperate grasslands. *Theoretical and Applied Climatology* 140: 1093–1105.
- Vitasse Y, Baumgarten F, Zohner CM, Kaewthongrach R, Fu YH, Walde MG, Moser B. 2021. Impact of microclimatic conditions and resource availability on spring and autumn phenology of temperate tree seedlings. *New Phytologist* 232: 537–550.
- Wang H, Wang H, Ge Q, Dai J. 2020a. The interactive effects of chilling, photoperiod, and forcing temperature on flowering phenology of temperate woody plants. *Frontiers in Plant Science* 11: 443.
- Wang H, Wu C, Ciais P, Peñuelas J, Dai J, Fu Y, Ge Q. 2020b. Overestimation of the effect of climatic warming on spring phenology due to misrepresentation of chilling. *Nature Communications* 11: 2156.
- Wang X, Guo Z, Zhang K, Fu Z, Lee CKF, Yang D, Detto M, Zhang Y, Wu J. 2025. Can large-scale satellite products track the effects of atmospheric dryness and soil water deficit on ecosystem productivity under droughts? *Geophysical Research Letters* 20: 110785.
- White MA, de Beurs KM, Didan K, Inouye DW, Richardson AD, Jensen OP, O'keefe J, Zhang G, Nemani RR, van Leeuwen WJ *et al.* 2009. Intercomparison, interpretation, and assessment of spring phenology in North America estimated from remote sensing for 1982–2006. *Global Change Biology* 15: 2335–2359.
- Winkler K, Fuchs R, Rounsevell MD, Herold M. 2020. HILDA+ Global Land Use Change between 1960 and 2019. *Pangaea*. doi: [10.1594/PANGAEA.921846](https://doi.org/10.1594/PANGAEA.921846).
- Wu C, Peng J, Ciais P, Peñuelas J, Wang H, Beguería S, Andrew Black T, Jassal RS, Zhang X, Yuan W *et al.* 2022. Increased drought effects on the phenology of autumn leaf senescence. *Nature Climate Change* 12: 943–949.
- Wu Z, Lin C-F, Wang S, Gong Y, Fu YH, Tang J, De Boeck HJ, Vitasse Y, Zhao Y-P. 2022. The sensitivity of ginkgo leaf unfolding to the temperature

- and photoperiod decreases with increasing elevation. *Agricultural and Forest Meteorology* 315: 108840.
- Xie Y, Wilson AM. 2020. Change point estimation of deciduous forest land surface phenology. *Remote Sensing of Environment* 240: 111698.
- Yan Z, Guo Z, Serbin SP, Song G, Zhao Y, Chen Y, Wu S, Wang J, Wang X, Li J *et al.* 2021. Spectroscopy outperforms leaf trait relationships for predicting photosynthetic capacity across different forest types. *New Phytologist* 232: 134–147.
- Yang Y, Chen R, Yin G, Wang C, Liu G, Verger A, Descals A, Filella I, Peñuelas J. 2022. Divergent performances of vegetation indices in extracting photosynthetic phenology for northern deciduous broadleaf forests. *IEEE Geoscience and Remote Sensing Letters* 19: 1–5.
- Zeng Z-G, Beck PS, Wang T-J, Skidmore AK, Song Y-L, Gong H-S, Prins HH. 2010. Effects of plant phenology and solar radiation on seasonal movement of golden takin in the Qinling Mountains, China. *Journal of Mammalogy* 91: 92–100.
- Zhang X, Friedl MA, Schaaf CB, Strahler AH, Hodges JCF, Gao F, Reed BC, Huete A. 2003. Monitoring vegetation phenology using MODIS. *Remote Sensing of Environment* 84: 471–475.
- Zhang J, Tong X, Zhang J, Meng P, Li J, Liu P. 2021. Dynamics of phenology and its response to climatic variables in a warm-temperate mixed plantation. *Forest Ecology and Management* 483: 118785.
- Zhang X, Friedl M, Henebry G. 2020. VIIRS/NPP land cover dynamics yearly L3 global 500m SIN grid V001. NASA EOSDIS Land Processes DAAC.
- Zhao H, Fu YH, Wang X, Zhang Y, Liu Y, Janssens IA. 2021. Diverging models introduce large uncertainty in future climate warming impact on spring phenology of temperate deciduous trees. *Science of the Total Environment* 757: 143903.
- Zhou Z, Zhang L, Liu Y, Zhang K, Wang W, Zhu J, Chai S, Zhang H, Miao Y. 2022. Contrasting effects of nitrogen addition on vegetative phenology in dry and wet years in a temperate steppe on the Mongolian Plateau. *Frontiers in Plant Science* 13: 861794.

Supporting Information

Additional Supporting Information may be found online in the Supporting Information section at the end of the article.

Fig. S1 Distribution of Köppen climate classification within the study area.

Fig. S2 Performance comparison of the OPT-S-VPD, OPT-S, and OPT-VPD models against the original OPT model in predicting plant spring phenology across different plant functional types.

Fig. S3 Linear regression analysis between the heterogeneity using two metrics and RMSE.

Table S1 Distribution and percentage of Köppen climate zones within our study area.

Please note: Wiley is not responsible for the content or functionality of any Supporting Information supplied by the authors. Any queries (other than missing material) should be directed to the *New Phytologist* Central Office.

Disclaimer: The New Phytologist Foundation remains neutral with regard to jurisdictional claims in maps and in any institutional affiliations.